LETTER

doi:10.1038/nature22051

Super-multiplex vibrational imaging

Lu Wei[1], Zhixing Chen[1], Lixue Shi[1], Rong Long[1], Andrew V. Anzalone[1], Luyuan Zhang[1], Fanghao Hu[1], Rafael Yuste[2,3,4], Virginia W. Cornish[1,2] & Wei Min[1,2,4]

The ability to visualize directly a large number of distinct molecular species inside cells is increasingly essential for understanding complex systems and processes. Even though existing methods have successfully been used to explore structure–function relationships in nervous systems, to profile RNA *in situ*, to reveal the heterogeneity of tumour microenvironments and to study dynamic macromolecular assembly[1–4], it remains challenging to image many species with high selectivity and sensitivity under biological conditions. For instance, fluorescence microscopy faces a 'colour barrier', owing to the intrinsically broad (about 1,500 inverse centimetres) and featureless nature of fluorescence spectra[5] that limits the number of resolvable colours to two to five (or seven to nine if using complicated instrumentation and analysis)[6–8]. Spontaneous Raman microscopy probes vibrational transitions with much narrower resonances (peak width of about 10 inverse centimetres) and so does not suffer from this problem, but weak signals make many bio-imaging applications impossible. Although surface-enhanced Raman scattering offers high sensitivity and multiplicity, it cannot be readily used to image specific molecular targets quantitatively inside live cells[9]. Here we use stimulated Raman scattering under electronic pre-resonance conditions to image target molecules inside living cells with very high vibrational selectivity and sensitivity (down to 250 nanomolar with a time constant of 1 millisecond). We create a palette of triple-bond-conjugated near-infrared dyes that each displays a single peak in the cell-silent Raman spectral window; when combined with available fluorescent probes, this palette provides 24 resolvable colours, with the potential for further expansion. Proof-of-principle experiments on neuronal co-cultures and brain tissues reveal cell-type-dependent heterogeneities in DNA and protein metabolism under physiological and pathological conditions, underscoring the potential of this 24-colour (super-multiplex) optical imaging approach for elucidating intricate interactions in complex biological systems.

Stimulated Raman scattering (SRS) microscopy, which was developed for label-free imaging of chemical bonds, uses nonlinear Raman effects to accelerate weak vibrational transitions by 10^8 times in the far field (Extended Data Fig. 1) and thereby overcomes the sensitivity or biocompatibility limitations of other Raman imaging modalities[10,11]. Coupling SRS with strong vibrational tags such as alkynes (C≡C) allows effective imaging of diverse biomolecules[12–15], but detection sensitivity is limited to about 15 mM for typical chemical bonds such as C–H and 200 μM for the stronger C≡C bond, leaving many targets (such as metabolites, proteins, RNA and organelles) out of reach[10–13].

These sensitivity limits are associated with SRS microscopy being operated in the non-resonance region, with the pump laser energy (ω_{pump}) well below the molecular absorption peak energy (ω_0) (Fig. 1a). Electronic resonance is known to greatly enhance Raman signals[16], and moving from non-resonance ($\omega_0 \gg \omega_{pump}$) to rigorous resonance ($\omega_0 = \omega_{pump}$) indeed enhances the detected stimulated Raman loss signal (apparent pump intensity decrease) of the near-infrared dye IR895 by a factor of about 10^8 compared to the C–O vibrational signal from methanol (compare purple and yellow spectra in Fig. 1a). But this signal boost comes with a large decrease in chemical specificity: the desired narrow-band vibrational signatures of IR895 are almost overwhelmed by the concurrent broad background that possibly originates from a combination of electronic-resonance four-wave mixing processes and competing pump–probe processes[17].

We hypothesized that carefully adjusted detuning might retain signal enhancement and improve the contrast between vibrational signal and electronic background. A moderate detuning to $\omega_0 - \omega_{pump} \approx 2\Gamma$ (where Γ is the homogeneous linewidth, typically about 700 cm^{-1}) results in the electronic pre-resonance SRS (epr-SRS) spectrum of another near-infrared dye Cy7.5 starting to present an observable peak from the conjugated C=C bonds, with a ratio of vibrational signal to electronic background (S/B) of 0.5 (Fig. 1a, cyan spectrum). Further detuning to around 3Γ gives rise to a clean epr-SRS peak in the spectrum of the dye ATTO740, with vanishing electronic background (Fig. 1a, blue spectrum). A pre-resonance enhancement factor of 2×10^5 is achieved for this conjugated C=C bond when compared to C–O in methanol, a magnitude comparable to previous reports for resonance Raman spectroscopy[18]. The epr-SRS detection limit of ATTO740 by targeting this peak is determined to be 250 nM, with a time constant of 1 ms (Fig. 1b). This corresponds to about 30–40 molecules within the focal volume, which is about 1,000 times more sensitive than the previous record for non-resonance SRS imaging[12] and comparable to that for confocal fluorescence microscopy, while retaining distinct vibrational contrast.

In our first proof-of-principle epr-SRS microscopy demonstration, we image ATTO740-labelled 5-ethynyl-2′-deoxyuridine (EdU)—a metabolic target for newly synthesized DNA—in HeLa cells with a short pixel dwell time of 4 μs (0.4 s per 320 × 320 frame) (Fig. 1c). The imaging pattern shows high resemblance to the corresponding fluorescence contrast pattern (Extended Data Fig. 2a). Owing to the narrow vibrational resonance, the epr-SRS signal disappears when the pump laser wavelength λ_{pump} is off-resonance by only 2 nm (Fig. 1d), demonstrating very high chemical selectivity that is unattainable with fluorescence (Extended Data Fig. 3a–d). The epr-SRS signal retains 97% of its initial value even after 100 frames of continuous imaging (Fig. 1e, Extended Data Fig. 2b), indicating photo-stability in the pre-resonance region.

To demonstrate the versatility of epr-SRS imaging, we imaged the ATTO740 immuno-labelled intracellular proteins α-tubulin (which has clearly resolved tubule structures; Fig. 1f) and Tom20 (a mitochondria receptor; Fig. 1g), and the ATTO740 immuno-labelled membrane receptor of tumour marker keratin 18 (Fig. 1h); see Extended Data Fig. 2c, d for additional examples. In addition to immuno-labelling, epr-SRS imaging of genetically encoded H2B proteins in live cells was achieved using a commercially available self-labelling protein tag (SNAP-tag) with far-red silicon-rhodamine (SiR) dye (Fig. 1i). Organelle targets (Fig. 1j) and chemical drugs (Fig. 1k) can also be visualized in live cells, using MitoTracker deep red and methylene blue (a widely used drug and a photosensitizer in photodynamic therapy

[1]Department of Chemistry, Columbia University, New York, New York 10027, USA. [2]NeuroTechnology Center, Columbia University, New York, New York 10027, USA. [3]Departments of Biological Sciences and Neuroscience, Columbia University, New York, New York 10027, USA. [4]Kavli Institute for Brain Science, Columbia University, New York, New York 10032, USA.

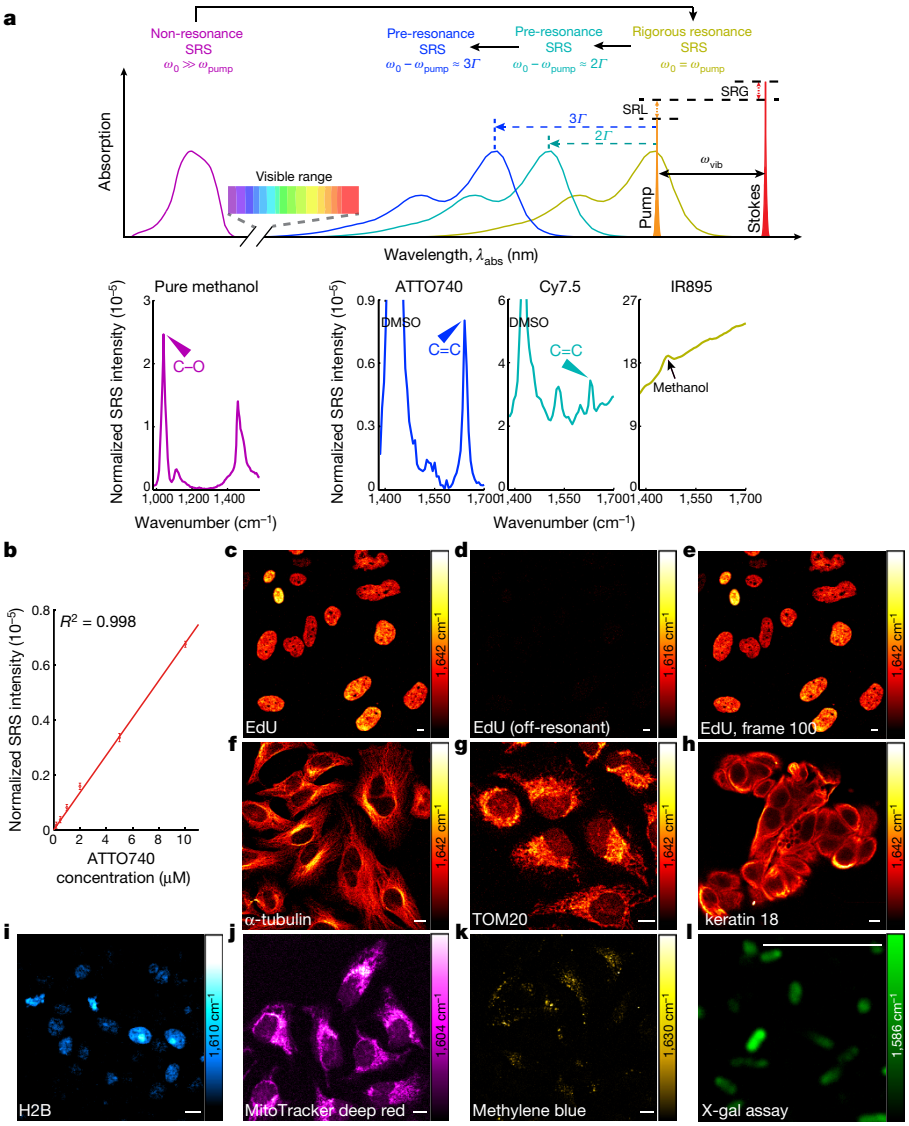

Figure 1 | Electronic pre-resonance stimulated Raman scattering (epr-SRS) microscopy. a, Different SRS regimes, which are defined by the difference in energy between the molecular absorption peak (ω_0) and the pump laser (ω_{pump}): non-resonance ($\omega_0 \gg \omega_{pump}$; purple), pre-resonance ($\omega_0 - \omega_{pump} \approx 3\Gamma$ or 2Γ, where $\Gamma \approx 700\,cm^{-1}$ is the homogeneous linewidth; blue and cyan) and rigorous resonance ($\omega_0 = \omega_{pump}$; yellow). The Stokes wavelength (red pulse) is fixed at 1,064 nm and the pump wavelength (orange pulse) is tuned between 850 nm and 960 nm for the corresponding vibrational transitions (ω_{vib}) of the chemical bonds. The stimulated Raman loss (SRL; relative to the laser input level) is detected as signals (Extended Data Fig. 1); the stimulated Raman gain (SRG) is also indicated. Representative SRS spectra are shown below for each regime: pure methanol (about 25 M) at non-resonance, IR895 (2.5 μM) at rigorous resonance ($\lambda_{abs} \approx 900$ nm, methanol), and Cy7.5 (50 μM, $\lambda_{abs} \approx 800$ nm, DMSO) and ATTO740 (50 μM, $\lambda_{abs} \approx 760$ nm, DMSO) at pre-resonance. The C–O band in the non-resonance regime and the C=C bands in the pre-resonance regimes are indicated by arrow-heads; solvent bands are also marked. **b**, Linear dependence of epr-SRS signals on ATTO740 concentration (C=C at 1,642 cm^{-1}) with a 1-ms time constant. Error bars, mean ± s.d. **c**, Fast epr-SRS imaging of ATTO740-labelled 5-ethynyl-2′-deoxyuridine (EdU) by click-chemistry for newly synthesized DNA in HeLa cells. **d**, **e**, Off-resonance image (**d**) and the 100th image frame (**e**) for the same set of cells shown in **c**. **f**–**g**, epr-SRS imaging of ATTO740 immuno-labelled α-tubulin (**f**) and Tom20 (**g**) in HeLa cells, and keratin 18 in MCF7 cells (**h**). **i**–**l**, epr-SRS imaging of SiR-SNAP-tagged, genetically encoded H2B proteins (**i**), MitoTracker deep red (**j**) and methylene blue (**k**) in live HeLa cells, and oxidation product 4,4′-dichloro-5,5′-dibromoindigo from X-gal hydrolysis in *E. coli* (**l**). Scale bars, 10 μm. In **c**–**l**, the number inside each colour scale denotes the targeted vibrational on-resonance peak wavenumber for epr-SRS imaging, with the colour indicating the amplitude of the signal at that wavenumber.

that is probably enriched in lysosomes), respectively. Finally, to demonstrate utility in a small-molecule-based functional assay, we monitored the production of a non-fluorescent indigo product from a classic *lacZ* gene-expression assay in live *E. coli* (Fig. 1l).

We next focused on developing an epr-SRS reporter dye palette. By characterizing 28 commercial dyes across a wide range of ω_0 (Fig. 2a, Extended Data Table 1), we confirmed that their Raman scattering cross-sections (σ(C=C)) increase steeply as ω_0 approaches ω_{pump}. This trend can be fitted quantitatively to the Albrecht A-term pre-resonance approximation, using a single fitting parameter K (Fig. 2a, red line):

$$\sigma = K\omega_{pump}(\omega_{pump} - \omega_{vib})^3 \left[\frac{\omega_{pump}^2 + \omega_0^2}{(\omega_0^2 - \omega_{pump}^2)^2}\right]^2$$

where ω_{vib} is the vibrational transition energy and K is a collection of frequency-independent factors of the dyes[16,19]. We therefore defined an optimal epr-SRS excitation region as $2\Gamma < \omega_0 - \omega_{pump} < 6\Gamma$ (Fig. 2a, grey shading) to ensure both chemical specificity ($S/B > 0.5$) and sensitivity (<5 μM with a 1-ms time constant). Within this near-infrared region

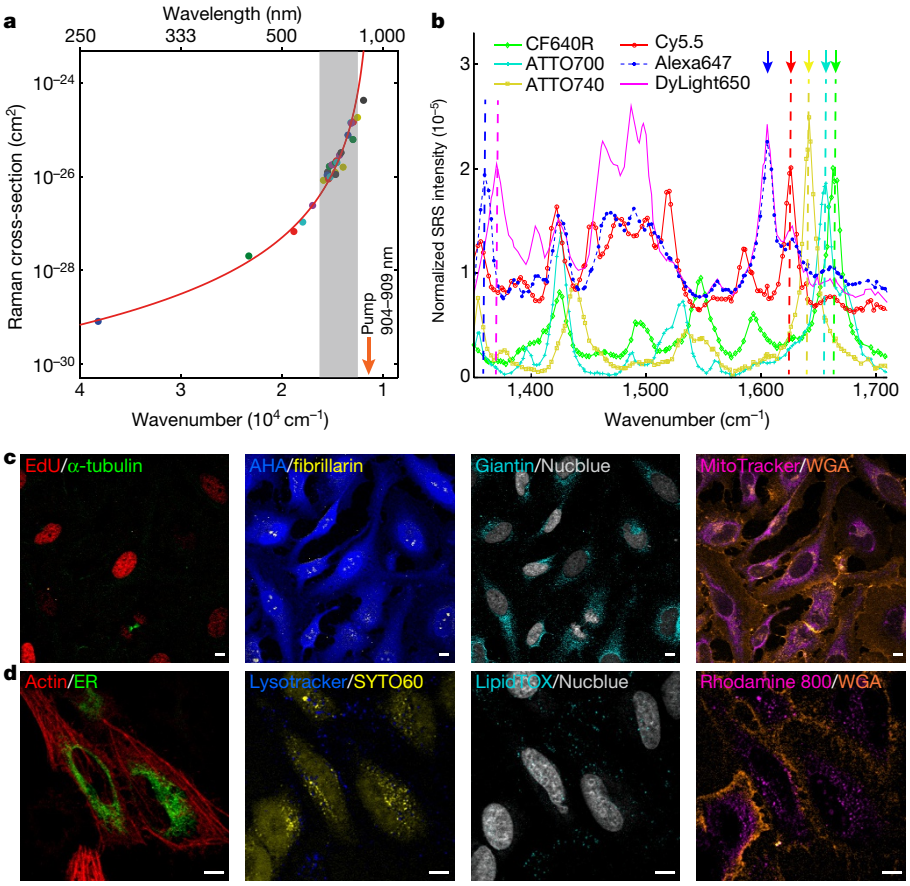

Figure 2 | Multiplex epr-SRS imaging with commercial dyes in fixed and live mammalian cells. a, Semi-logarithmic plot of the measured Raman cross-sections for conjugated C=C bonds of 28 organic dyes (coloured circles) across a wide range of absorption-peak energies (excited by $\lambda_{pump} = 904–909$ nm (orange arrow)). The grey-shaded area indicates the defined epr-SRS region. The 28 data points are fitted (red curve) using the Albrecht A-term pre-resonance approximation equation. **b**, Resolvable epr-SRS spectra of six commercial dyes, with the peaks corresponding the C=C vibrations indicated by vertical dashed lines: CF640R (300 μM, 1,665 cm^{-1}), ATTO700 (100 μM, 1,657 cm^{-1}), ATTO740 (80 μM, 1,642 cm^{-1}), Cy5.5 (250 μM, 1,626 cm^{-1}), Alexa647 (500 μM, 1,606 cm^{-1} and 1,359 cm^{-1}) and DyLight650 (500 μM, 1,606 cm^{-1} and 1,370 cm^{-1}). Occasional residual backgrounds (for example, for DyLight650) are probably from two-photon absorption. **c**, Eight-colour epr-SRS (of channels indicted by arrow in **b**) and fluorescence imaging in fixed HeLa cells. epr-SRS: EdU (newly synthesized DNA, Cy5.5, red), α-tubulin (bundles in cytokinesis, CF640R, green), azidohomoalaine (AHA; newly synthesized proteins, Alexa647, blue), fibrillarin (nucleoli marker, ATTO740, yellow) and giantin (Golgi marker, ATTO700, cyan). Fluorescence: Nucblue (total DNA, grey), wheat-germ agglutinin (WGA; glycoproteins, Alexa488, orange) and MitoTracker orange (mitochondria marker, magenta). **d**, Eight-colour imaging in live Hela cells. epr-SRS: Lysotracker (lysosome marker, blue), SYTO60 (nucleic acid stain, yellow), LipidTOX deep red (neutral lipid stain, cyan), WGA (glycoproteins, ATTO740, orange) and rhodamine 800 (mitochondria marker, magenta). Fluorescence: actin (red fluorescent protein, red), endoplasmic reticulum (ER; green fluorescent protein, green) and Nucblue (total DNA, grey). Scale bars, 10 μm.

(approximately 650–800 nm), six commercial dyes with largely overlapping fluorescence (Extended Data Fig. 3e), but mutually resolvable epr-SRS spectra (Fig. 2b, dash-lined), were identified as multiplexable reporters for the epr-SRS palette.

We then selected five C=C peaks to demonstrate the multiplex imaging capability (Fig. 2b, arrowed). Spectral cross-talks are minimized using a linear-combination algorithm (see Methods). We further noted that the epr-SRS imaging in the near-infrared is orthogonal to fluorescence detection in the visible region (the non-resonance SRS region), so merging epr-SRS and fluorescent palettes enabled imaging with eight different colours (five quantitative epr-SRS of C=C bonds and three fluorescence channels) of the same set of fixed cells (Fig. 2c, Extended Data Fig. 4). Combining fluorescent proteins in the visible region with commercial organelle trackers in the epr-SRS region also enabled eight-colour imaging of live cells (Fig. 2d), a feat difficult to achieve by other means.

The epr-SRS dye palette can be expanded further, especially when going beyond conjugated C=C bonds and targeting triple bonds such as alkynes (C≡C) and nitriles (C≡N) that display a single sharp Raman peak in the wide silent window (1,800–2,800 cm^{-1})[12–15,20]. The challenge here is that the triple bonds must be coupled with an electronic transition to enable pre-resonance enhancement, which will depend sensitively on the electronic–vibrational coupling strength[16]. Hence, simply installing a triple bond onto an arbitrary position of a dye will most often not yield satisfying signals.

We rationally designed a new library of near-infrared dyes (Fig. 3a), in which nitrile or alkyne triple bonds directly participate in the π-conjugation systems of the molecule, with xanthene identified as a promising scaffold[21,22] after initial screening. To generate more vibrational colours, we used three combined strategies guided by the classical $\omega_{vib} \propto \sqrt{k/\mu}$ equation, where k is a spring constant that reflects the bond strength and $\mu = m_1 m_2/(m_1 + m_2)$ is the reduced mass. As illustrated in Fig. 3a, substituting the 10-position of xanthene from O to C or Si (ref. 23; green), gradually expanding the xanthene rings (yellow) and modifying the terminal groups for alkyne dyes (purple) all fine-tune the triple-bond strength by affecting the electron-density of the π-conjugation system. Combinatorial isotopic editing of the two atoms involved in the triple bond (Fig. 3a, red and blue) enables local modulation of their reduced mass into four possible combinations[24] that further expand the vibrational palette.

We synthesized most of the dyes (including their ^{13}C and ^{15}N isotopologues) in our conceived library (Fig. 3a), referring to promising

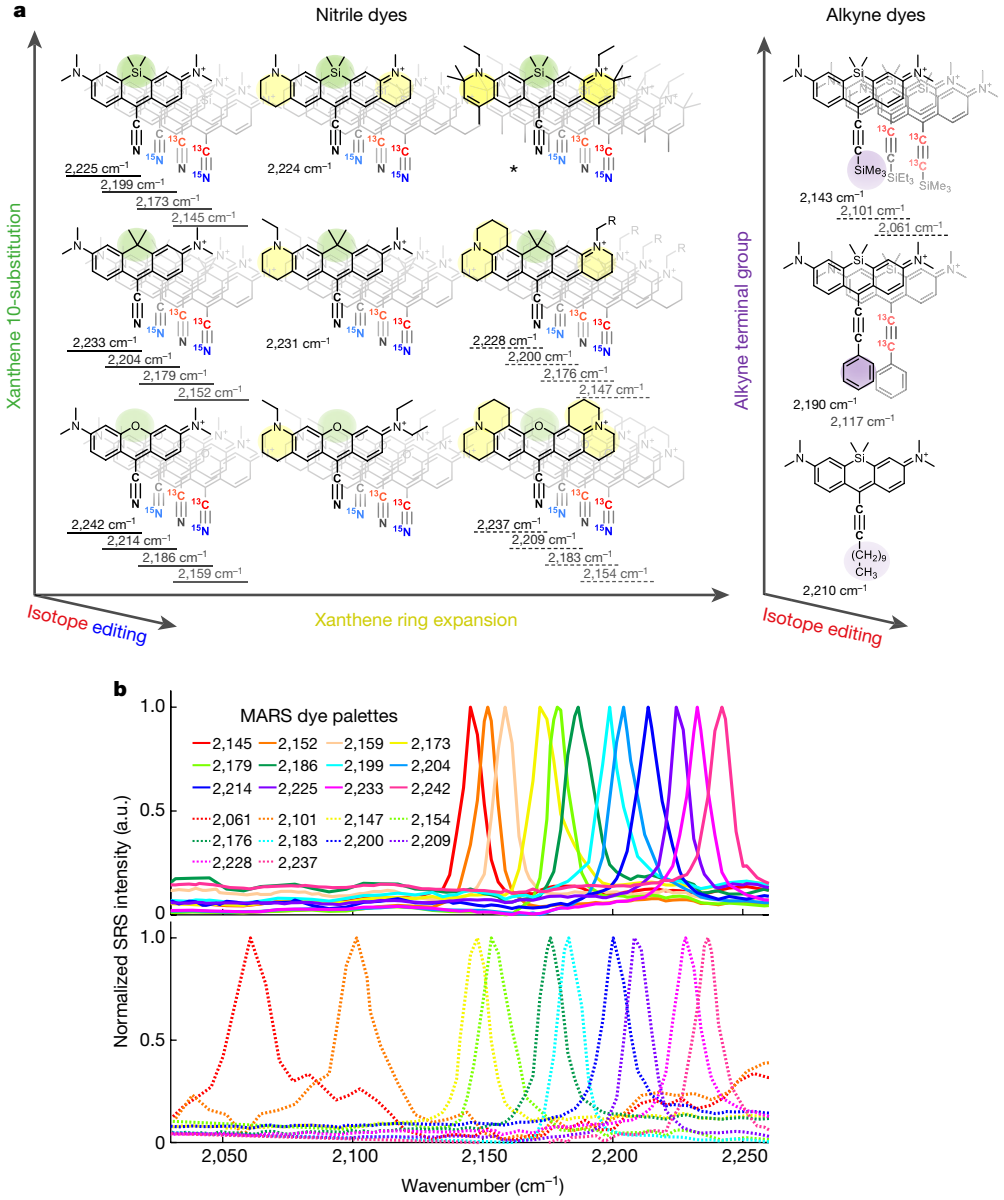

Figure 3 | Manhattan Raman scattering (MARS) dyes bearing π-conjugated, isotopically edited, electronically fine-tuned triple bonds. a, Design principles and structures for a three-dimensional library of epr-SRS nitrile (left) and alkyne (right) dyes. The axes in each panel indicate different strategies for modifying the dye structure to fine-tune the vibrational frequencies; the corresponding modifications in the structures are colour-coded. *Dyes with overwhelming background due to close electronic resonance. **b**, Two sets of MARS palettes and their normalized epr-SRS spectra in the cell-silent window. The upper panel shows 12 MARS dyes, whose vibrational frequencies (in cm^{-1}) are indicated by numbers after solid lines, and are solid-underlined in **a**. The lower panel shows 10 MARS dyes, whose vibrational frequencies (in cm^{-1}) are indicated by numbers after dashed lines, and are dash-underlined in **a**.

structures with mutually resolvable epr-SRS peaks as Manhattan Raman scattering (MARS) dyes (synthesis procedures in Supplementary Information). We selected two sets of MARS palettes (selected structures are underlined in Fig. 3a), which together provide up to 14 well-resolved epr-SRS colours in the cell-silent window (Fig. 3b, Extended Data Table 2), and with all dyes displaying good specificity ($S/B > 5$) and sensitivity (<5 μM with 1-ms time constant). With the six commercial dyes in the Raman fingerprint region, our expanded vibrational palette consists of 20 resolvable reporters in the near-infrared. Combining this vibrational palette with four more fluorescence channels that are typically obtainable in the visible region allows us to access 24 colours for optical super-multiplexing.

Our epr-SRS vibrational palette has biocompatibility that ensures sufficient cell viability (Extended Data Fig. 5), the required photostability (Extended Data Fig. 6) and effective linear unmixing (Extended Data Fig. 7) to enable proof-of-principle imaging on live HeLa cells. After being separately stained with individual dyes and then mixed together, these cells are subjected to 16-colour live-cell imaging, which quadruples the number of colour channels that is typically achieved by fluorescence alone. The resultant image (Fig. 4a) was acquired through sequential imaging in 15 min, but further system development should enable simultaneous imaging. We then used this super-multiplexing technique to probe metabolic activity in complex nervous systems consisting of multiple cell types, under either physiological or pathological conditions. First, we used eight-colour imaging to image DNA replication and protein synthesis activities—two crucial processes in neural development and function—in hippocampal neuronal cultures (Fig. 4b, Extended Data Fig. 8a) and organotypic cerebellar tissues (Fig. 4c, Extended Data Fig. 8b), revealing highly heterogeneous DNA synthesis. We identified two newly divided cells (EdU^+) in neuronal

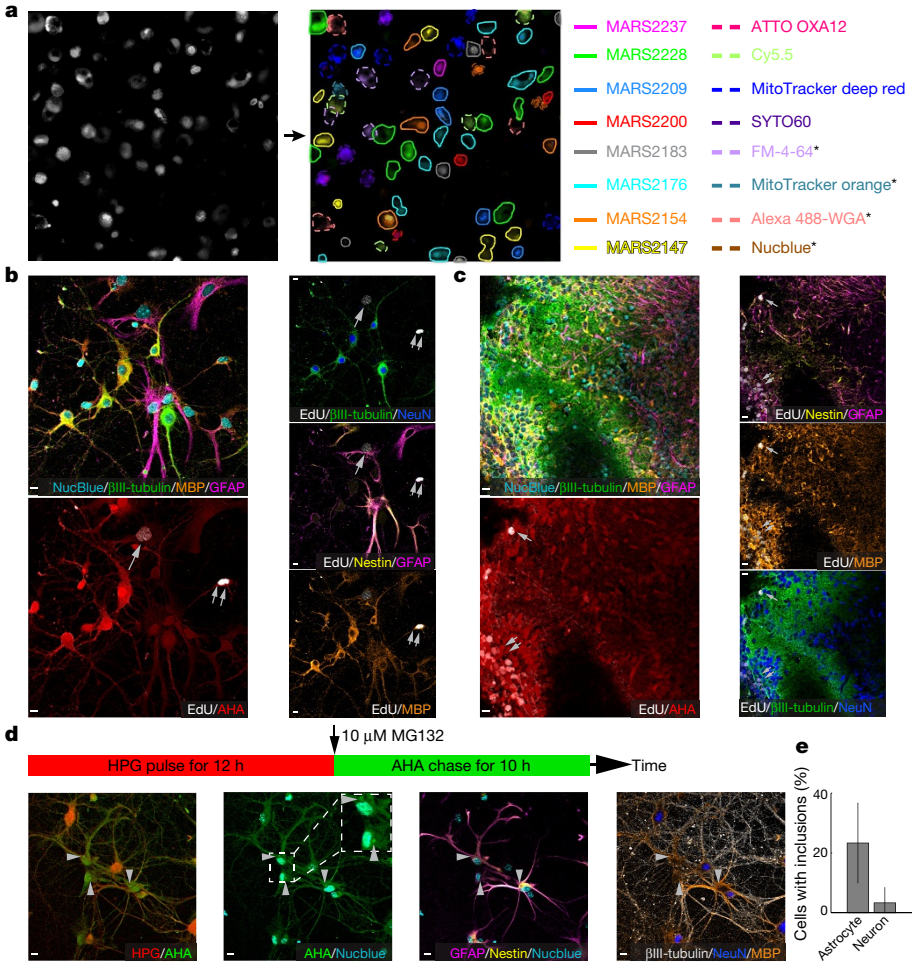

Figure 4 | Super-multiplex optical microscopy and its applications for probing metabolic activity in nervous systems under physiological and pathological conditions. a, Sixteen-colour live-cell imaging with eight MARS dyes, the four commercial vibrational dyes in the fingerprint and four additional fluorescent dyes (indicated by asterisks). Each pre-stained cell in the cell mix (grey image, left) is circled with the line colour and style (dashed or solid) matching that of the corresponding dye in the legend and shape (16-colour image, right). **b**, **c**, Eight-colour epr-SRS imaging of DNA replication and protein synthesis in hippocampal neuronal cultures (**b**) and organotypic cerebellar brain slices (**c**). Cells with newly synthesized DNA are indicated by arrows. **d**, Pulse–chase (HPG–AHA) imaging of proteome turnover dynamics in hippocampal neuronal cultures with proteasome inhibitor MG132 (10 μM) in the chase period (arrow). Aggregations are indicated by arrow heads. **e**, Percentages of the astrocyte and neuron cells in **d** that contain protein inclusions. Error bars, mean ± s.d., based on imaging $n = 6$ samples (see also Methods), with $P < 0.01$ determined using a two-sided Student's t-test. epr-SRS: β III-tubulin (neurons, MARS2200, green in **b**, **c**, grey in **d**), myelin basic protein (MBP; oligodendrocytes, MARS2176, orange), glial fibrillary acidic protein (GFAP; astrocytes and neural stem cells, MARS2147, magenta), EdU (newly synthesized DNA, MARS2228, grey in **b**, **c**), HPG (proteins synthesized in pulse period, MARS2228, red in **d**) and AHA (proteins synthesized in chase period, Alexa647, red in **b**, **c**, green in **d**). Fluorescence: Nucblue (total DNA, cyan), NeuN (neurons, Alexa568, blue) and nestin (neural stem cells and astrocytes, Alexa488, yellow). Scale bars, 10 μm.

co-cultures, after confirming labelling specificity for each channel (Fig. 4b, left). Multicolour cross-examination revealed that one was astrocytic (Fig. 4b, single arrows; as evidenced by present (+)/absent (−) protein markers βIII-tubulin$^-$, NeuN$^-$, nestin$^+$ and GFAP$^+$) and the other oligodendrocytic (Fig. 4b, double arrows; βIII-tubulin$^-$, NeuN$^-$, nestin$^-$, GFAP$^-$ and MBP$^+$). When imaging organotypic cerebellar tissues of P11 mice, we observed a high number of EdU$^+$ cells probably concentrated in the molecular layer (Fig. 4c, left), which might be a progenitor-cell niche (Fig. 4c, right, highlighted by arrows; nestin$^+$, MBP$^+$ and NeuN$^-$). These observations establish that our super-multiplex imaging platform is well suited for probing molecular heterogeneity in nervous systems.

We then studied neuronal systems under proteasomal stress. Proteostasis—the balance between synthesis of new proteins and degradation of aberrant proteins—is precisely regulated through cellular 'quality control', particularly the ubiquitin–proteasome system, with proteasome dysfunction implicated in many neurodegenerative diseases and ageing processes[25]. When studying individual cell types under proteasomal stress (modelled by applying proteasome inhibitor MG132), astrocytes were found to be more resistant than neurons and oligodendrocytes[26]. Because such cell-type-dependent vulnerability is unexplored in more realistic environments in which different cells co-exist, we used eight-colour imaging to study the global proteostasis stress in neuronal co-cultures with largely preserved astrocyte–neuron coupling. As expected, applying MG132 (Fig. 4d, top) retarded the proteome turnover (Extended Data Fig. 9). Obvious cytosolic proteome aggregations (inclusions) were observed in only the chase channel (Fig. 4d, bottom left), suggesting that newly synthesized proteins are more susceptible to proteasomal impairment and are prone to aggregation. This finding is consistent with the fact that up to 30% of newly synthesized proteins are misfolded[27]. Most importantly, subsequent cross-channel examination indicated that proteome inclusions appeared mostly in astrocytes instead of in neurons (Fig. 4d, bottom right; Fig. 4e). Considering that the formation of protein inclusions may exert a protective role by sequestering potentially harmful species from the cytosol[28], this result suggests that the astrocyte resistance

observed previously might be due to their ability to actively form protein inclusions that sequester the toxic misfolded species, whereas neurons are unable to do so.

Although the above proof-of-principle observations already demonstrate the potential of our technique, it can be further improved along multiple fronts. First, the MARS dye palette can potentially be expanded to 50 or more colours by filling the rather broad cell-silent window with individual sharp peaks from new vibrational moieties. Second, genetically encoded infrared proteins could be engineered to serve as vibrational reporters[29]. Third, hyper-spectral imaging[30] could be implemented to realize faster and simultaneous signal acquisition. Given these expected further improvements, and because our technique offers sensitivity, resolution, labelling versatility and biocompatibility that approach or are similar to those of fluorescence microscopy, we expect it to find wide application in the probing of complex systems.

Online Content Methods, along with any additional Extended Data display items and Source Data, are available in the online version of the paper; references unique to these sections appear only in the online paper.

Received 21 September 2016; accepted 3 March 2017.
Published online 19 April 2017.

1. Lichtman, J. W. & Denk, W. The big and the small: challenges of imaging the brain's circuits. *Science* **334,** 618–623 (2011).
2. Chen, K. H., Boettiger, A. N., Moffitt, J. R., Wang, S. & Zhuang, X. RNA imaging. Spatially resolved, highly multiplexed RNA profiling in single cells. *Science* **348,** aaa6090 (2015).
3. Giesen, C. *et al.* Highly multiplexed imaging of tumour tissues with subcellular resolution by mass cytometry. *Nat. Methods* **11,** 417–422 (2014).
4. Shroff, H. *et al.* Dual-color superresolution imaging of genetically expressed probes within individual adhesion complexes. *Proc. Natl Acad. Sci. USA* **104,** 20308–20313 (2007).
5. Lakowicz, J. R. *Principles of Fluorescence Spectroscopy* 3rd edn (Springer, 2011).
6. Dean, K. M. & Palmer, A. E. Advances in fluorescence labelling strategies for dynamic cellular imaging. *Nat. Chem. Biol.* **10,** 512–523 (2014).
7. Tsurui, H. *et al.* Seven-color fluorescence imaging of tissue samples based on Fourier spectroscopy and singular value decomposition. *J. Histochem. Cytochem.* **48,** 653–662 (2000).
8. Niehörster, T. *et al.* Multi-target spectrally resolved fluorescence lifetime imaging microscopy. *Nat. Methods* **13,** 257–262 (2016).
9. Lane, L. A., Qian, X. & Nie, S. SERS nanoparticles in medicine: from label-free detection to spectroscopic tagging. *Chem. Rev.* **115,** 10489–10529 (2015).
10. Min, W., Freudiger, C. W., Lu, S. & Xie, X. S. Coherent nonlinear optical imaging: beyond fluorescence microscopy. *Annu. Rev. Phys. Chem.* **62,** 507–530 (2011).
11. Cheng, J.-X. & Xie, X. S. Vibrational spectroscopic imaging of living systems: an emerging platform for biology and medicine. *Science* **350,** aaa8870 (2015).
12. Wei, L. *et al.* Live-cell imaging of alkyne-tagged small biomolecules by stimulated Raman scattering. *Nat. Methods* **11,** 410–412 (2014).
13. Hong, S. *et al.* Live-cell stimulated Raman scattering imaging of alkyne-tagged biomolecules. *Angew. Chem. Int. Ed.* **53,** 5827–5831 (2014).
14. Yamakoshi, H. *et al.* Imaging of EdU, an alkyne-tagged cell proliferation probe, by Raman microscopy. *J. Am. Chem. Soc.* **133,** 6102–6105 (2011).
15. Weeks, T., Wachsmann-Hogiu, S. & Huser, T. Raman microscopy based on doubly-resonant four-wave mixing (DR-FWM). *Opt. Express* **17,** 17044–17051 (2009).
16. Asher, S. A. UV resonance Raman studies of molecular structure and dynamics: applications in physical and biophysical chemistry. *Annu. Rev. Phys. Chem.* **39,** 537–588 (1988).
17. McCamant, D. W., Kukura, P. & Mathies, R. A. Femtosecond broadband stimulated Raman: a new approach for high-performance vibrational spectroscopy. *Appl. Spectrosc.* **57,** 1317–1323 (2003).
18. Le Ru, E. C. & Etchegoin, P. G. Single-molecule surface-enhanced Raman spectroscopy. *Annu. Rev. Phys. Chem.* **63,** 65–87 (2012).
19. Albrecht, A. C. & Hutley, M. C. On the dependence of vibrational Raman intensity on the wavelength of incident light. *J. Chem. Phys.* **55,** 4438–4443 (1971).
20. Yamakoshi, H. *et al.* Alkyne-tag Raman imaging for visualization of mobile small molecules in live cells. *J. Am. Chem. Soc.* **134,** 20681–20689 (2012).
21. Shi, J., Zhang, X.-P. & Neckers, D. C. Xanthenes: flourone derivatives II. *Tetrahedron Lett.* **34,** 6013–6016 (1993).
22. Pastierik, T., Šebej, P., Medalová, J., Štacko, P. & Klán, P. Near-infrared fluorescent 9-phenylethynylpyronin analogues for bioimaging. *J. Org. Chem.* **79,** 3374–3382 (2014).
23. Koide, Y. *et al.* Development of NIR fluorescent dyes based on Si-rhodamine for *in vivo* imaging. *J. Am. Chem. Soc.* **134,** 5029–5031 (2012).
24. Chen, Z. *et al.* Multicolor live-cell chemical imaging by isotopically edited alkyne vibrational palette. *J. Am. Chem. Soc.* **136,** 8027–8033 (2014).
25. Kaushik, S. & Cuervo, A. M. Proteostasis and aging. *Nat. Med.* **21,** 1406–1415 (2015).
26. Jänen, S. B., Chaachouay, H. & Richter-Landsberg, C. Autophagy is activated by proteasomal inhibition and involved in aggresome clearance in cultured astrocytes. *Glia* **58,** 1766–1774 (2010).
27. Goldberg, A. L. Protein degradation and protection against misfolded or damaged proteins. *Nature* **426,** 895–899 (2003).
28. Chen, B., Retzlaff, M., Roos, T. & Frydman, J. Cellular strategies of protein quality control. *Cold Spring Harb. Perspect. Biol.* **3,** a004374 (2011).
29. Shu, X. *et al.* Mammalian expression of infrared fluorescent proteins engineered from a bacterial phytochrome. *Science* **324,** 804–807 (2009).
30. Liao, C.-S. *et al.* Spectrometer-free vibrational imaging by retrieving stimulated Raman signal from highly scattered photons. *Sci. Adv.* **1,** e1500738 (2015).

Supplementary Information is available in the online version of the paper.

Acknowledgements We thank L. Brus and A. McDermott for discussions, M. Jimenez and C. Dupre for suggestions, and L. Shi for technical assistance. W.M. acknowledges support from an NIH Director's New Innovator Award (1DP2EB016573), R01 (EB020892), the US Army Research Office (W911NF-12-1-0594), the Alfred P. Sloan Foundation and the Camille and Henry Dreyfus Foundation. R.Y. is supported by the NEI (EY024503, EY011787) and NIMH (MH101218, MH100561).

Author Contributions L.W. carried out the spectroscopy, microscopy and biological studies together with L.S. and with the help of L.Z., F.H. and R.Y.; Z.C. designed and performed chemical synthesis together with R.L., A.V.A. and L.W. under the guidance of V.W.C. and W.M.; L.W. and W.M. conceived the concept; and L.W., Z.C. and W.M. wrote the manuscript with input from all authors.

Author Information Reprints and permissions information is available at www.nature.com/reprints. The authors declare competing financial interests: details are available in the online version of the paper. Readers are welcome to comment on the online version of the paper. Publisher's note: Springer Nature remains neutral with regard to jurisdictional claims in published maps and institutional affiliations. Correspondence and requests for materials should be addressed to W.M. (wm2256@columbia.edu).

Reviewer Information *Nature* thanks C. H. Camp Jr and T. Huser for their contribution to the peer review of this work.

METHODS

Stimulated Raman scattering (SRS) microscopy. An integrated laser (picoEMERALD with custom modification, Applied Physics and Electronics, Inc.) was used as a light source for both pump and Stokes beams. Briefly, picoEMERALD provided an output pulse train at 1,064 nm with 6-ps pulse width and 80-MHz repetition rate, which served as the Stokes beam. The frequency-doubled beam at 532 nm was used to synchronously seed a picosecond optical parametric oscillator (OPO) to produce a mode-locked pulse train (the idler beam of the OPO was blocked with an interferometric filter) with 5–6-ps pulse width. The wavelength of the OPO was tunable from 720 nm to 990 nm, which served as the pump beam. The intensity of the 1,064 nm Stokes beam was modulated sinusoidally by a built-in electro-optic modulator (EOM) at 8 MHz with a modulation depth of more than 95%. The pump beam was spatially overlapped with the Stokes beam with a dichroic mirror inside picoEMERALD. The temporal overlap between pump and Stokes pulse trains was ensured with a built-in delay stage and optimized by the SRS signal of deuterium oxide (99.9 at% D, 151882 ALDRICH).

Pump and Stokes beams were coupled into an inverted laser-scanning microscope (FV1200MPE, Olympus) optimized for near-infrared throughput. A 25× water objective (XLPlan N, 1.05 numerical aperture (NA), MP, Olympus) with high near-infrared transmission and large field of view was used for measurements of all solutions, cells and tissues unless otherwise specified. A 60× water objective (UPlanAPO/IR, 1.2 NA, Olympus) with high near-infrared transmission was used for the X-gal assay and live-cell 8-colour imaging. The pump/Stokes beam size was matched to fill the back-aperture of the corresponding objectives for imaging. The forward-going pump and Stokes beams after passing through the samples were collected in transmission with a high-NA condenser lens (oil immersion, 1.4 NA, Olympus), which was aligned following Köhler illumination. A telescope was then used to image the scanning mirrors onto a large-area (10 mm × 10 mm) Si photodiode (FDS1010, Thorlabs) to descan beam motion during laser scanning. The photodiode was reverse-biased by 64 V from a DC power supply to increase the saturation threshold and the response bandwidth. A high-optical-density bandpass filter (890/220 CARS, Chroma Technology) was used to block the Stokes beam completely and transmit the pump beam only. The output current of the photodiode was electronically pre-filtered by an 8-MHz band-pass filter (KR 2724, KR electronics) to suppress the 80-MHz laser pulsing and the low-frequency contribution due to laser scanning across the scattering sample. It was then fed into a radio-frequency lock-in amplifier (SR844, Stanford Research Systems or HF2LI, Zurich instrument), terminated with 50 Ω to demodulate the stimulated Raman loss signal experienced by the pump beam. The in-phase X-output of the lock-in amplifier was fed back into the analogue interface box (FV10-ANALOGUE) of the microscope.

All laser powers were measured after the objective lens. For the spectroscopy measurement in Fig. 1, the Stokes laser power was $P_{\text{Stokes}} = 18.4$ mW. For the detection sensitivity measurement, pump and Stokes laser powers were $P_{\text{pump}} = 24$ mW and $P_{\text{Stokes}} = 184$ mW, respectively. For the cellular and tissue imaging, the range of laser powers used were $P_{\text{pump}} = 7$–24 mW and $P_{\text{Stokes}} = 46$–120 mW. Pixel dwell times for all images ranged from 4 μs (0.4 s per 320 × 320 frame; Fig. 1c–e) to 200 μs (20.5 s per 320 × 320 frame; Figs 2c, d, 4b–d). The time constants of the lock-in amplifier were chosen to be about two times shorter than the pixel dwell time. All fluorescence images were acquired using a commercial Olympus FV1200MPE microscope equipped with 488-nm, 543-nm and 633-nm continuous-wave lasers. Two-photon fluorescence was excited by the tunable pump laser at designated wavelengths and detected by non-descanned photomultiplier tubes. For two-photon fluorescence imaging of Nucblue (Figs. 2 and 4), the two-photon fluorescence was excited by an OPO laser at 780 nm, and the fluorescence was detected after passing through a 690-nm short-pass filter, reflected by a 570-nm long-pass dichroic and then through a 450/40-nm band-pass filter (Thorlabs, FB450-40). The detections for two-photon fluorescence signals of Nucblue in the ultraviolet/blue and of epr-SRS in the near-infrared are still orthogonal to each other with no issue of signal overlapping. For two-photon fluorescence imaging of Alexa647 (Extended Data Fig. 3c, d), the two-photon fluorescence is excited by an OPO laser at around 810 nm, and the fluorescence was detected after passing through a 690-nm short-pass filter and a 570-nm long-pass dichroic.

SRS spectra acquisition. SRS spectra for all dyes were acquired by fixing the Stokes beam at 1,064 nm and scanning the pump beam through the designated wavelength range point by point.

Linear-combination algorithm. Because epr-SRS signals depend linearly on analyte concentrations, different dyes with overlapping Raman bands may be quantitatively distinguished using a simple and robust linear-combination algorithm. The measured N-channel epr-SRS signals ($\boldsymbol{S}$) for N dyes is expressed as the product of a $N \times N$ Raman cross-section matrix (M) and dye concentrations ($\boldsymbol{C}$), with the addition of the cellular amide backgrounds in each channel ($\boldsymbol{B}$): $\boldsymbol{S} = M\boldsymbol{C} + \boldsymbol{B}$, where

$$\boldsymbol{C} = [C_{\text{dye1}}, \ldots, C_{\text{dye}N}]^{\text{T}}$$

$$\boldsymbol{S} = [S_{\text{channel1}}, \ldots, S_{\text{channel}N}]^{\text{T}}$$

$$\boldsymbol{B} = [B_{\text{channel1}}, \ldots, B_{\text{channel}N}]^{\text{T}}$$

$$M = \begin{bmatrix} \sigma_{\text{dye1,channel1}} & \cdots & \sigma_{\text{dye}N\text{,channel1}} \\ \vdots & \ddots & \vdots \\ \sigma_{\text{dye1,channel}N} & \cdots & \sigma_{\text{dye}N\text{,channel}N} \end{bmatrix}$$

Dye concentrations were therefore determined using $\boldsymbol{C} = M^{-1}(\boldsymbol{S} - \boldsymbol{B})$. For epr-SRS in the fingerprint region (Fig. 2c, d), $\boldsymbol{B}$ was obtained by acquiring a reference image at the label-free channel of 2,940 cm^{-1} for total proteins, and then scaling it to the amide backgrounds in individual epr-SRS channels. The scaling factors were determined in reference HeLa cells without labels under the corresponding imaging conditions. For MARS dyes (Fig. 4), $\boldsymbol{B}$ was vanishing and the equation becomes $\boldsymbol{C} = M^{-1}\boldsymbol{S}$. The algorithm was implemented in Matlab.

Protein labelling with dye NHS esters. *Conjugation to secondary antibodies.* *N*-hydroxysuccinimide (NHS) ester-activated dyes were dissolved in DMSO to a concentration of 2 mg ml^{-1}. Secondary antibodies were dissolved or diluted to 2 mg ml^{-1} in PBS and adjusted with a sodium bicarbonate buffer to a final pH of 8.3. For purchased antibodies with concentrations lower than 2 mg ml^{-1}, proteins were first concentrated with Amicon ultra-centrifugal filters (UFC501096, EMD, Millipore). A 50-μl dye–NHS solution was slowly added to a 0.5-ml protein solution. The reaction was incubated at room temperature for 60 min under constant but slow stirring. The labelled proteins could be separated from unreacted dye NHS esters by gel permeation chromatography with Sephadex G-25 (G25150 SIGMA) packed in a column, which has a diameter of around 1 cm and a length of more than 12 cm. Sephadex G-25 was first swelled in PBS in a 90 °C water bath for 1 h. After the gel settled at room temperature, the buffer was exchanged for fresh PBS and gels were stored at 4 °C. For gel chromatography, the column was packed with swelled gels and then equilibrated with PBS. The labelled protein solution was then loaded and eluted with PBS. The first eluted band, which shows a light colour for dye-conjugated proteins, was collected. This solution was then centrifuged and supernatant was collected and concentrated with Amicon ultra-centrifugal filters (UFC501096, EMD, Millipore) into a final concentration of 1–2 mg ml^{-1} in PBS with 30% glycerol and 5 mM sodium azide, and stored at −20 °C.

Conjugation to wheat-germ agglutinin (WGA, L0636 SIGMA). All procedures were the same as those described above, except the dye-protein ratio: a 17.5-μl dye–NHS solution with a concentration of 2 mg ml was slowly added to a 0.5-ml WGA solution with a concentration of 2 mg ml^{-1}.

Sample information. All samples were made into imaging chambers using an imaging spacer (GBL654008 SIGMA) between a coverslip and a microscope slide. The chamber was filled with PBS for imaging. All imaging results were experimentally replicated more than five times.

Cell lines. Cell lines were purchased from ATCC: HeLa (ATCC CCL-2), MCF7 (ATCC HTB-22) and HEK 293T/17 (ATCC CRL-11268). These cell lines were authenticated and mycoplasma-negative. The cell medium was made of 90% Dulbecco's modified Eagle medium (DMEM; 11965, invitrogen), 10% fetal bovine serum (FBS; 10082, invitrogen) and 1× penicillin/streptomycin (15140, invitrogen). The methionine-deficient DMEM medium was made by supplying 4 mM L-glutamine, 0.2 mM L-cystine, 10% FBS and 1× penicillin/streptomycin to DMEM without L-methionine, L-cysteine and L-glutamine (D0422 SIGMA).

Mice and tissues. The animal experimental protocol (AC-AAAQ2457) was approved by the Institutional Animal Care and Use Committee at Columbia University. 400-μm-thick cerebellar brain slices from P11 wild-type (C57BL/6) mice of either sex were cultured with methionine-deficient brain-slice culture medium containing 1 mM AHA and 100 μM EdU for 17 h. Organotypic slices were then fixed with 4% paraformaldehyde (PFA) for 30 min, followed with 0.5% Triton permeabilization overnight at 4 °C. No statistical methods were used to predetermine sample size. All experimental procedures were performed in a non-blinded manner and no randomization was applied.

Antibodies. Primary antibodies for single-colour labelling: anti-fibrillarin antibody, nucleolar marker in rabbit (ab5821, Abcam); anti-200 kD neurofilament heavy antibody in rabbit (ab8135, Abcam); anti-α-tubulin antibody in rabbit (ab18251, Abcam); anti-Tom20 antibody in rabbit (sc-11415, Santa Cruz Biotechnology); anti-giantin antibody in rabbit (ab24586, Abcam); anti-cytokeratin 18 antibody in mouse (ab7797, Abcam); anti-CD44 antibody in mouse (ab6124, Abcam); anti-EpCAM antibody in rabbit (ab71916, Abcam); and anti-IGF1 receptor β subunit antibody in mouse (ab80547, Abcam). For multicolour labelling: anti-fibrillarin antibody, nucleolar marker in mouse (ab4566, Abcam); anti-α-tubulin antibody in chicken (ab89984, Abcam); anti-giantin antibody in rabbit (ab24586, Abcam); anti-βIII-tubulin in chicken (ab107216, Abcam); anti-myelin basic protein in mouse (ab62631, Abcam); anti-GFAP in goat (ab53554, Abcam); anti-nestin in

rat (ab81462, Abcam); and anti-NeuN in rabbit (ab177487, Abcam). Secondary antibodies: goat-anti-rabbit ATTO740 antibody (49559, Sigma); goat-anti-mouse ATTO740 antibody (2111, Hypermol); goat-anti-rabbit ATTO700 antibody (2310, Hypermol); goat anti-chicken CF640R antibody (20084, Biotium); donkey-anti-rabbit Alexa568 (ab175692, Abcam); and donkey-anti-rat Alexa488 (ab150153, Abcam). Donkey-anti-mouse (Sigma, SAB3701101), donkey-anti-chicken (Invitrogen, SA172002) and donkey-anti-goat (Sigma, G6638) antibodies were conjugated with MARS dyes.

Dyes. Most dyes are listed in Extended Data Table 1. Others are ATTO740 NHS ester (59808 SIGMA) and IR895 (392375 SIGMA).

Experimental procedures for epr-SRS imaging. *Imaging newly synthesized DNA in HeLa cells by metabolic incorporation of 5-ethynyl-2′-deoxyuridine (EdU, T511285, Aldrich) and detection with ATTO740-azide.* See Fig. 1c–e and Extended Data Fig. 2a, b. HeLa cells were seeded on a coverslip in a Petri dish with DMEM for 20 h, then replaced with DMEM medium without FBS for another 20 h for synchronization. 10 μM EdU in fresh DMEM medium was then added to cells for 15 h. Cell were fixed with 4% PFA for 20 min and permeabilized with 0.5% Triton for 10 min. 1 μM ATTO740-azide (AD 740-101, ATTO-TEC) in Click-iT cell reaction buffer (C10269, Invitrogen) was then added to cells to react with EdU for 20 min. Cells were washed twice with PBS before imaging.

Immuno-staining for single-colour epr-SRS imaging of fixed HeLa or MCF7 cells. See Fig. 1f–h and Extended Data Fig. 2c, d. HeLa/MCF7 cells were seeded on a coverslip in a Petri dish with 2 ml of DMEM for 20 h, and then fixed with 4% PFA for 20 min or methanol for 25 min. After fixation, cells were washed with 10% goat serum/1% bovine serum albumin (BSA)/0.3 M glycine solution twice before permeabilization in 0.1% Tween PBS for 40 min. Primary antibody was subsequently added by 1:200 dilution in 3% BSA at 4 °C overnight. After blocking with 10% goat serum for 30 min, secondary antibody conjugated with fluorophores was added by 1:100 dilution in 10% goat serum at 4 °C overnight. The samples were blocked with 10% goat serum for 30 min before imaging.

epr-SRS imaging of SiR SNAP-tagged H2B proteins. See Fig. 1i. HEK293T cells were seeded on a coverslip in a Petri dish with DMEM for 20 h before being transfected with 250 ng SNAP-H2B plasmid (New England BioLabs) for 48 h. 10 μM SNAP-SiR (S9102S, New England BioLabs) was then added to the medium for 45 min at 37 °C. Cells were washed three times with PBS before imaging.

epr-SRS imaging of MitoTracker deep red. See Fig. 1j. 500 nM MitoTracker deep red (M22426, Invitrogen) in Hank's balanced salt solution (HBSS) was added to cells for 20 min at 37 °C. Cells were washed twice with PBS before imaging.

epr-SRS imaging of methylene blue. See Fig. 1k. 10 μM methylene blue (M9140 SIGMA-ALDRICH) in PBS was added to cells for 20 min at 37 °C. Cells were washed twice with PBS before imaging.

epr-SRS imaging of the indigo product from the X-gal gene-expression assay. See Fig. 1l. BL21 *E. Coli* were grown in lysogeny broth (LB) medium to log phase before adding 100 μM X-gal (XGAL-RO ROCHE) and 1 mM isopropyl β-D-1-thiogalactopyranoside (IPTG; I6758 SIGMA-ALDRICH) for 20 min at 37 °C. *E. Coli* were then concentrated and washed with PBS before imaging.

8-colour epr-SRS and fluorescence imaging of fixed HeLa cells. See Fig. 2c. HeLa cells were seeded on a coverslip in a Petri dish with DMEM for 20 h, then replaced with methionine-deficient DMEM medium for 30 min. 1 mM L-azidohomoalanine (AHA, C10102, Invitrogen) and 100 μM EdU were then added into the medium for 18 h. 400 nM MitoTracker orange CMTMRos (M-7510, Invitrogen) was added into the medium for 30 min and 2 μM Alexa 488-WGA (W11261, Invitrogen) was added together for the last 15 min before fixation of the cells with 4% PFA for 8 min followed with methanol for 20 min. The subsequent immuno-staining procedures were that same as those described above. After secondary-antibody incubation, samples were blocked with 10% goat serum for 30 min. Then 5 μM Cy5.5-azide (178, AAT-Bioquest) with Click-iT cell reaction buffer was added to cells to react with EdU for 20 min. After washing with PBS, 2.5 μM Alexa 647-alkyne (A10278, Invitrogen) with Click-iT cell reaction buffer was added to cells to react with AHA for 20 min. Lastly, Nucblue Fixed Cell ReadyProbes reagent (R37606, Invitrogen) was added to cells for 10 min. Cells were washed with PBS before imaging.

8-colour epr-SRS and fluorescence imaging of live HeLa cells. See Fig. 2d. HeLa cells were first seeded on coverslips in Petri dishes with DMEM culture medium at 37 °C for 24 h. ER-GFP (C10590, Invitrogen) and actin-RFP (C10583, Invitrogen) plasmids were transfected into cells for 48 h following the protocol from Invitrogen. 500 μM oleic acid (O1383 SIGMA) coupled with BSA in DMEM culture medium was then added to cells for 7 h to induce the formation of lipid droplets. Before imaging, cells were first incubated with 6 μM SYTO60 (S11342, Invitrogen), 120 nM LysoTracker deep red (L12492, Invitrogen) and 400 nM rhodamine 800 (83701 SIGMA) in HBSS simultaneously for 30 min at 37 °C, followed by staining with Nucblue Live ReadyProbes reagent (R37605, Invitrogen) in HBSS for 20 min at 37 °C. Cells were then incubated with ATTO 740-conjugated WGA in HBSS for 30 min at 37 °C, followed by staining with LipidTOX deep red (H34477, Invitrogen) in HBSS with a dilution of 1:20 for 30 min at room temperature before imaging.

16-colour epr-SRS and fluorescence imaging of live HeLa cells. See Fig. 4a. HeLa cells were first seeded in a 24-well dish for 20 h. Each well of cells was labelled with a single colour of epr-SRS or fluorescent dye for 30 min in PBS: MARS2237 (1 μM), MARS2228 (4 μM), MARS2209 (1 μM), MARS2200 (4 μM), MARS2183 (1 μM), MARS2176 (4 μM), MARS2154 (1 μM), MARS2147 (4 μM), ATTO OXA12 (10 μM), Cy5.5 (2 μM), MitoTracker deep red (2.5 μM), SYTO60 (10 μM), FM 4-64 (T13320, Invitrogen, 20 μg ml^{-1}), MitoTracker orange (M7510, Invitrogen, 400 nM), Alexa488-WGA (W11261, Invitrogen, 2 μg ml^{-1}) or Nucblue (R37605, Invitrogen). Cells were then washed with PBS and detached from each well by trypsin treatment for 2 min, then mixed together in fresh DMEM medium before being gently centrifuged (1,000 r.p.m., 1.5 min) to pellet. PBS was added to the pellet and after gentle mixing, cells were sandwiched in the imaging chamber. Images were acquired after the cells had settled for 15–20 min on the imaging stage to reduce cell movement. Single-dye staining and a two-colour mix were first examined, and no cross-staining between cells was found during the imaging period (that is, each cell was maintained with a single pre-stained colour). We did not observe obvious stage drift during 16-colour image acquisitions. Figure 4a was acquired through sequential imaging in 15 min.

8-colour epr-SRS and fluorescence imaging of hippocampal neuronal cultures and cerebellar brain slices. See Fig. 4b-c. Regular hippocampal neuron medium was made of Neurobasal A medium (10888, Invitrogen), 1 × B27 serum-free supplement (17504, Invitrogen) and 0.5 mM glutamine (25030, Invitrogen). Methionine-deficient neuron medium was custom-made from a regular recipe of Neurobasal A medium (10888, Invitrogen) without methionine, and supplied with 1 × B27 serum-free supplement and 0.5 mM glutamine. Methionine-deficient medium for organotypic cerebellar brain slices was made by supplying methionine-deficient neuron medium with 1 × B27 serum-free supplement, 2 mM glutamine, 0.5% glucose and 1× penicillin/streptomycin.

Regular medium in D9 hippocampal neuronal cultures was first replaced by methionine-deficient medium containing 1 mM AHA and 100 μM EdU for 17 h. Cells were then fixed with 4% PFA for 20 min, followed with 0.5% Triton permeabilization for 15 min. Primary antibodies were then simultaneously added with 1:120 dilution in 3% BSA overnight at 4 °C. After blocking with 10% donkey serum for 30 min, secondary antibodies conjugated with fluorophores were added with 1:80 dilution in 10% donkey serum overnight at 4 °C. Samples were blocked with 10% donkey serum for 30 min with Nucblue Fixed Cell ReadyProbes reagent added for the last 10 min. 1 μM MARS2228-azide with Click-iT cell reaction buffer was the added to the cells or slices to react with EdU for 20 min. After washing with PBS, 12 μM Alexa 647-alkyne with Click-iT cell reaction buffer was added to react with AHA for 20 min. Cells were washed with PBS before imaging.

8-colour epr-SRS and fluorescence imaging in neuronal cultures. See Fig. 4d. Regular medium of D12 hippocampal neuronal cultures was replaced by methionine-deficient medium containing 1 mM L-homopropargylglycine (HPG; C10186, Invitrogen) for 12 h. The medium was then exchanged to fresh methionine-deficient medium containing 1 mM AHA with or without 10 μM MG132 (M7449 SIGMA) for another 10 h. Cells were fixed with 4% PFA for 20 min and then permeabilized with 0.5% Triton for 15 min. The immuno-staining procedures were the same as those described above. 1.25 μM MARS2228-azide with Click-iT cell reaction buffer was then added to the cells or slices to react with HPG for 20 min. After washing with PBS, 4 μM Alexa 647-alkyne with Click-iT cell reaction buffer was added to react with AHA for 20 min. Cells were washed with PBS before imaging.

Image statistics. See Fig. 4e. Six technical replicates of 8-colour images were acquired from three independent neuronal co-cultures (using the same conditions as described above for Fig. 4d) for statistical presentation. For each neuronal co-culture, two fields of view were selected close to the centre of the culture dish to maintain consistency. All images were taken under the same imaging parameters. Cross-checking 8-colour staining, the percentages of astrocytes and neurons with aggregations were calculated for each image set. Their means and standard deviations are presented in Fig. 4e, together with a *P* value from a two-sided Student's *t*-test.

Live/dead cell viability assay. See Extended Data Fig. 5. This assay was performed using the LIVE/DEAD viability/cytotoxicity kit for mammalian cells (Molecular Probes L-3224). HeLa cell standards and HeLa cells with dye staining or SRS pre-exposure were incubated with 2 μM calcein AM and 4 μM ethidium homodimer-1 (EthD-1) working solution for 20 min at 37 °C before imaging.

Data availability. All data that support this study are available from the corresponding author on request. Source Data for Fig. 4e are available in the online version of the paper.

31. Nima, Z. A. *et al.* Circulating tumor cell identification by functionalized silver-gold nanorods with multicolor, super-enhanced SERS and photothermal resonances. *Sci. Rep.* **9,** 4752 (2014).
32. Silva, W. R., Keller, E. L. & Frontiera, R. R. Determination of resonance Raman cross-sections for use in biological SERS sensing with femtosecond stimulated Raman spectroscopy. *Anal. Chem.* **86,** 7782–7787 (2014).

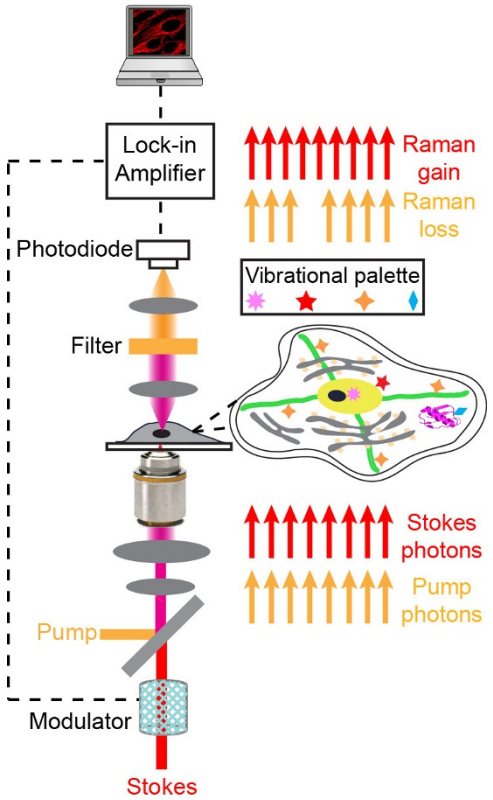

Extended Data Figure 1 | Apparatus of SRS microscopy. A narrow-band pump laser (5–6 ps pulse width) and an intensity-modulated Stokes laser (fixed at 1,064 nm, 6-ps pulse width) are temporally and spatially synchronized before collinearly focused onto cell samples. When the energy difference between the pump photons and the Stokes photons matches the vibrational frequency (ω_{vib}) of the targeted chemical bonds, the chemical bonds are efficiently excited to the vibrational excited state. For each transition, a photon in the pump beam is annihilated (stimulated Raman loss) and a photon in the Stokes beam is created (stimulated Raman gain). A lock-in detection scheme is used to sensitively measure the intensity loss of the pump beam (that is, stimulated Raman loss).

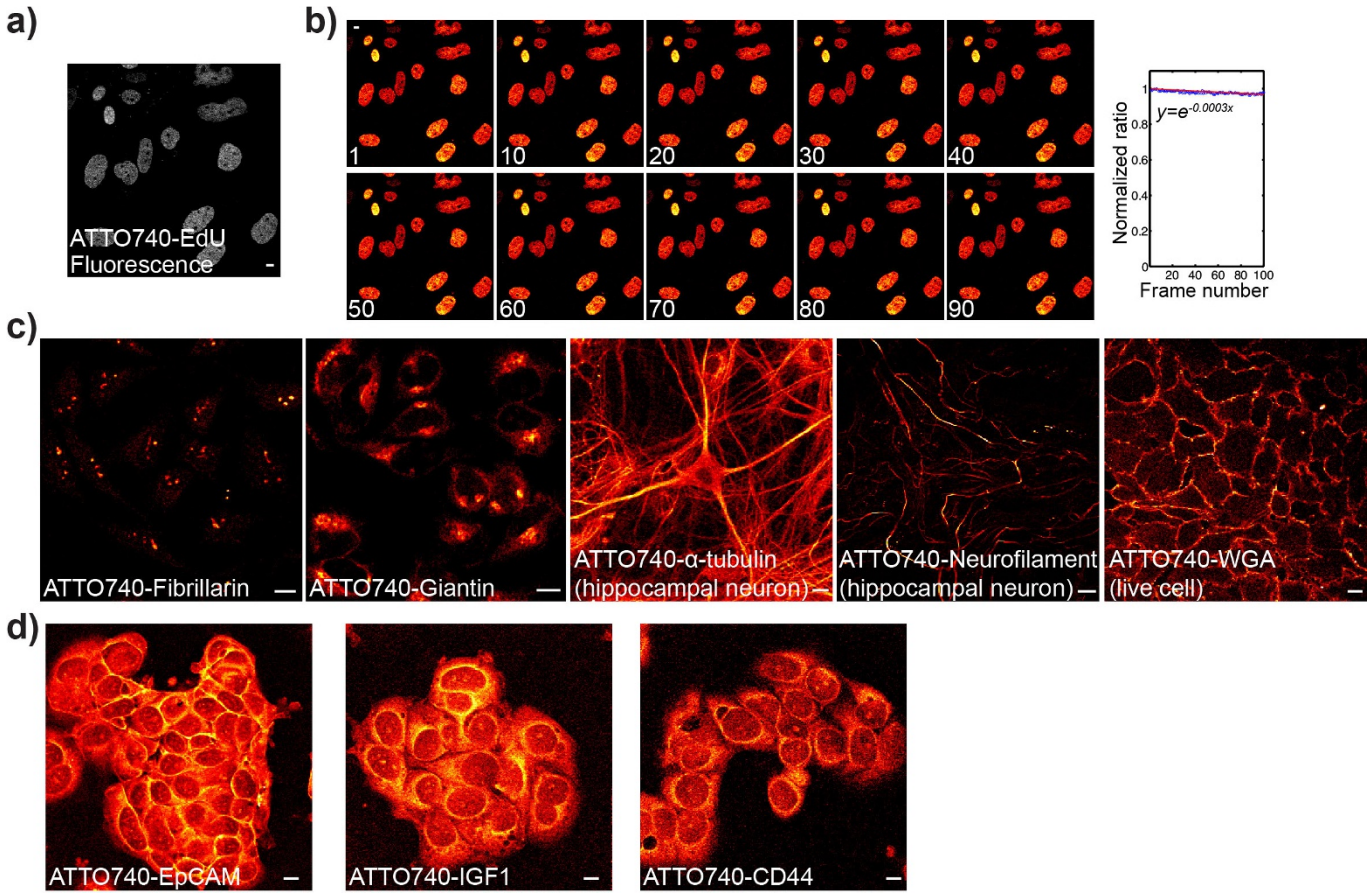

Extended Data Figure 2 | Sensitive epr-SRS imaging of ATTO740-labelled individual targets in HeLa, MCF7 and hippocampal neurons. **a**, Corresponding fluorescence image of ATTO740-labelled 5-ethynyl-2′-deoxyuridine (EdU) for newly synthesized DNA in the same cells as in Fig. 1c. **b**, Representative epr-SRS images of ATTO740-labelled EdU through continuous 100-frame imaging; frame numbers are indicated (left). Signal intensity curves are shown for imaging through 100 frames (right; data). The average photobleaching constant is determined to be 0.0003 (solid line). **c**, epr-SRS imaging of ATTO740 immuno-labelled fibrillarin (nucleolar marker) and giantin (Golgi membrane marker) in HeLa cells, α-tubulin and neurofilament (heavy, neuronal marker) in hippocampal neurons, and ATTO740-conjugated wheat-germ agglutinin (WGA), binded to membrane glycoproteins in live HeLa cells. **d**, epr-SRS imaging of ATTO740 immuno-labelled circulating tumour-cell markers[31]: epithelial cell adhesion molecule (EpCAM), insulin-like growth factor 1 (IGF1) and CD44. Scale bars, 10 μm.

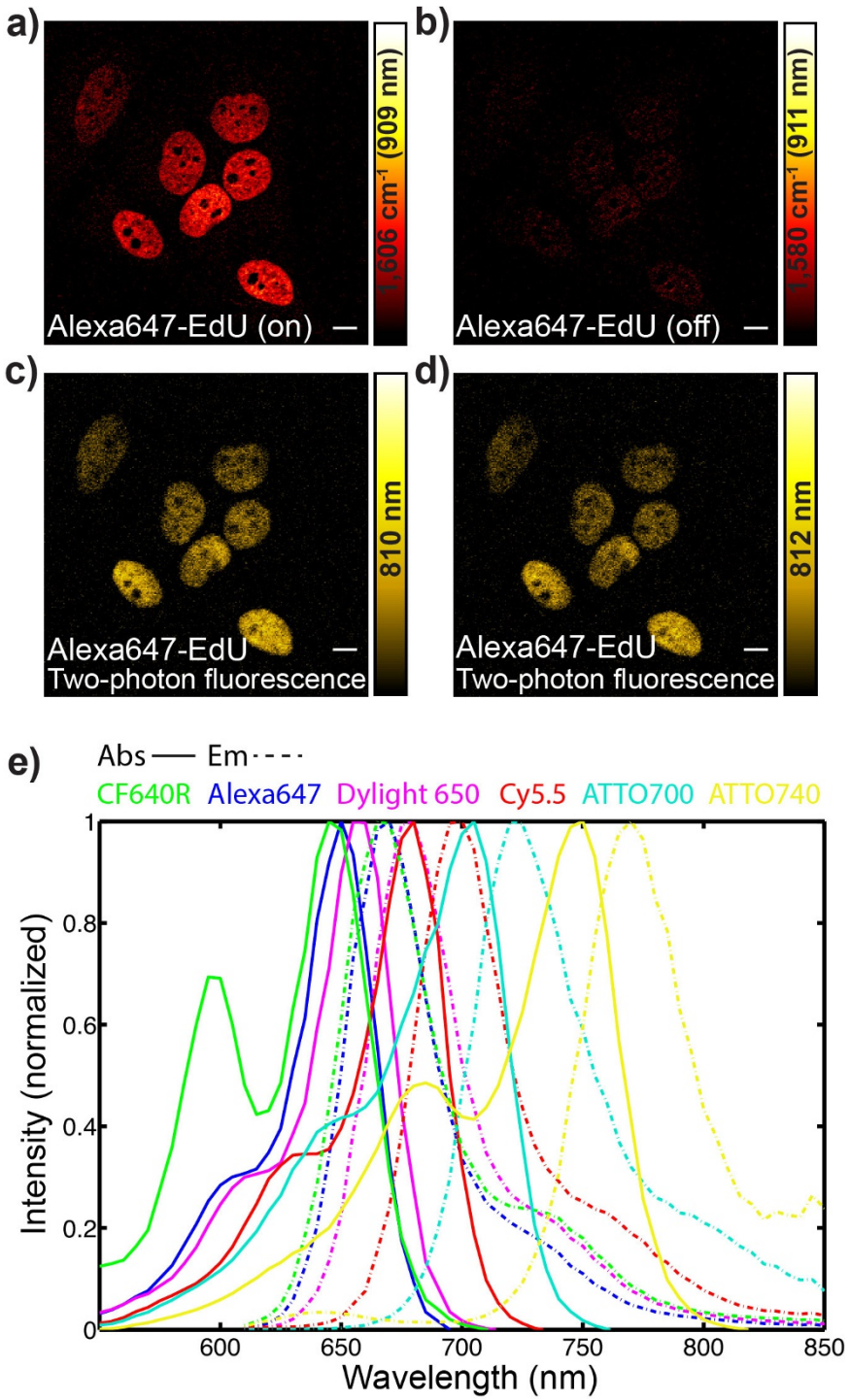

Extended Data Figure 3 | Chemical specificity comparison between epr-SRS and fluorescence imaging. a, On-resonance epr-SRS imaging of Alexa647-labelled EdU in HeLa cells at 1,606 cm^{-1} ($\lambda_{pump} = 909$ nm). **b**, Off-resonance image at 1,580 cm^{-1} ($\lambda_{pump} = 911$ nm) of the HeLa cells in **a**. **c**, **d**, Two-photon fluorescence images of the HeLa cells in **a** at 810 nm (**c**) and 812 nm (**d**) around the two-photon excitation peak of Alexa647. **e**, Absorption (solid) and emission (dashed) spectra for CF640R (green), Alexa647 (blue), DyLight650 (magenta), Cy5.5 (red), ATTO700 (cyan) and ATTO740 (yellow). Scale bars, 10 μm.

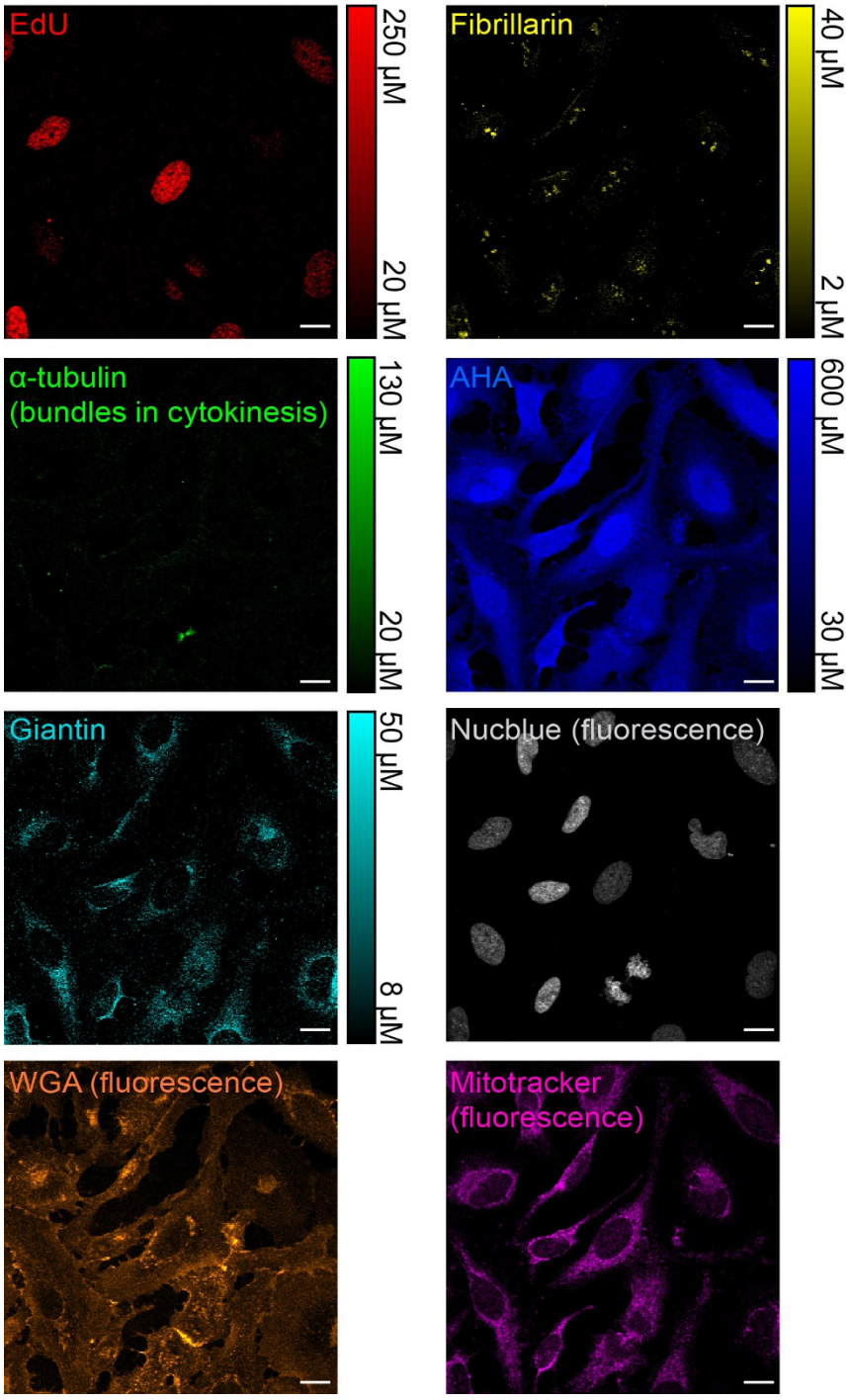

Extended Data Figure 4 | Quantitative epr-SRS and fluorescence imaging of non-overlaid images. Original images in Fig. 2c. Scale bars, 10 μm.

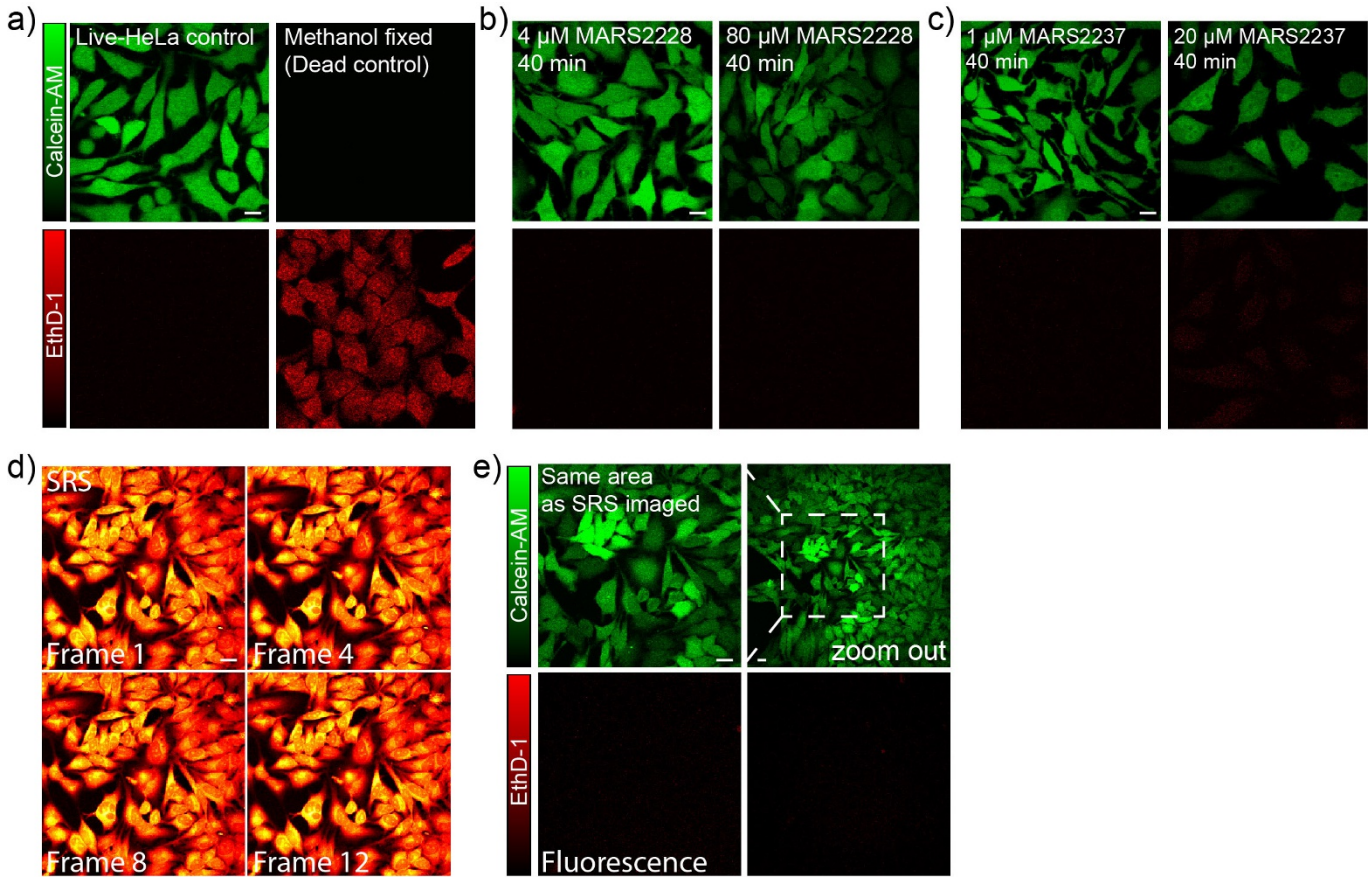

Extended Data Figure 5 | Minimum chemical toxicity of MARS dyes for multicolour live-cell imaging and photo-toxicity of SRS lasers. **a**, Control fluorescence images for live/dead cell-viability assay for live HeLa cells (calcein-AM, green, as live cell indicator) and fixed cells (EthD-1, red, as dead cell indicator). **b**, Live/dead cell-viability assay with 4 μM and 80 μM MARS2228-stained live cells did not reveal substantial chemical toxicity or cell death. 4 μM concentration is the same as used for live-cell stains in Fig. 4a; 80 μM with 20× concentration mimics the 20-colour staining conditions. This test would lead to the same results for MARS2200, MARS2176 and MARS2147, owing to the minimum chemical structural changes introduced by isotopic editing. **c**, Similar live/dead cell-viability assay with 1× and 20× concentration stain by MARS2237. This test would lead to the same results for MARS2209, MARS2183 and MARS2154. **d**, 12 continuous frames of SRS imaging targeting the vibrational peak of CH_3 (2,940 cm^{-1}) with the same laser power and dwell time as used for multiplex live-cell imaging. **e**, Fluorescence image of the set of pre-imaged cells in **d**. Live/dead cell-viability assay did not show observable cell death or any cell-viability loss when compared to the surrounding cells without pre-exposure to the SRS laser. Scale bars, 10 μm.

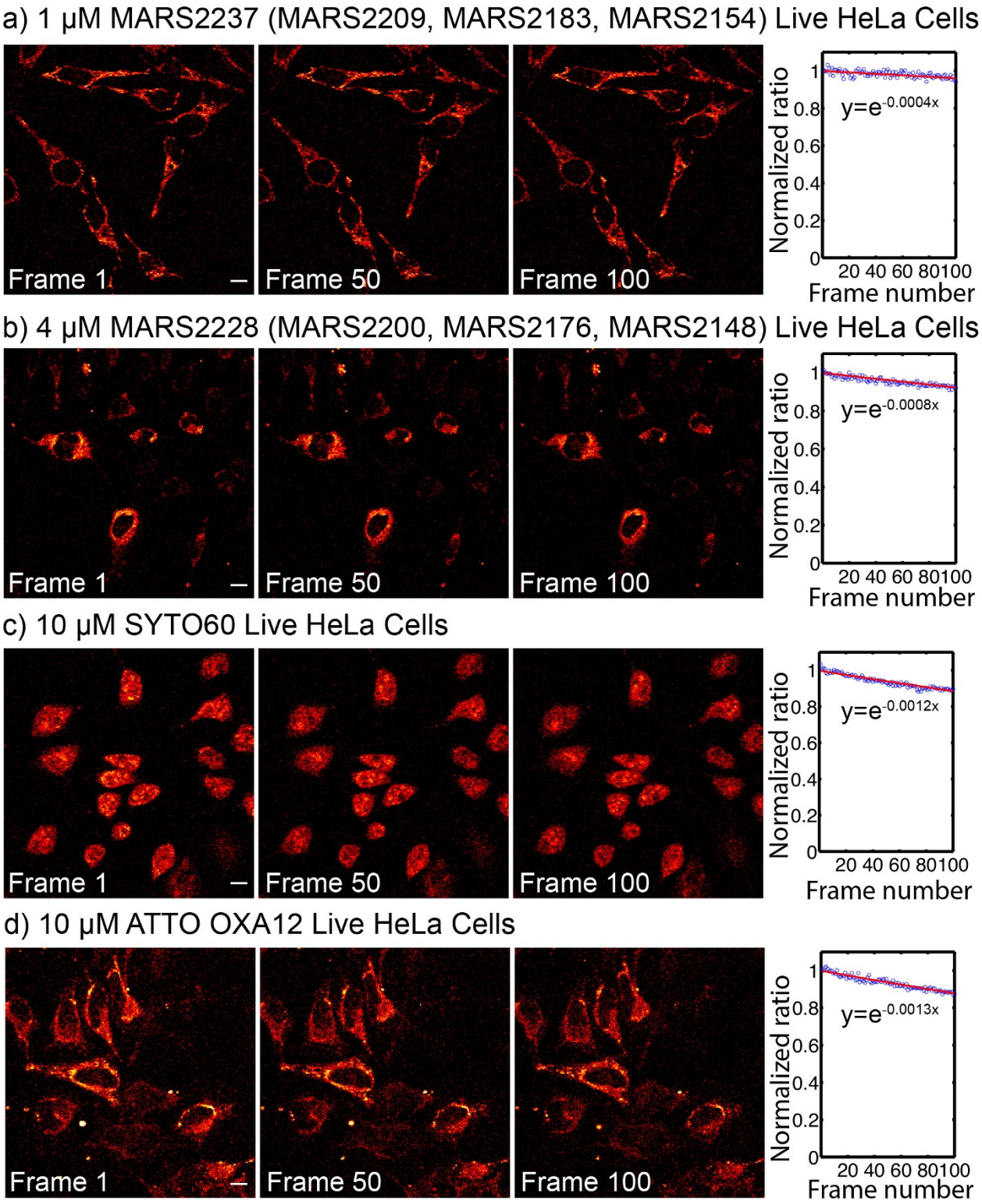

Extended Data Figure 6 | Photo-stability characterization for ten representative epr-SRS dyes (including eight MARS dyes) for live-cell imaging. **a–d**, The photo-bleaching percentage after 100 frames of SRS scans ranges from 4% to below 13%. Scale bars, 10 μm.

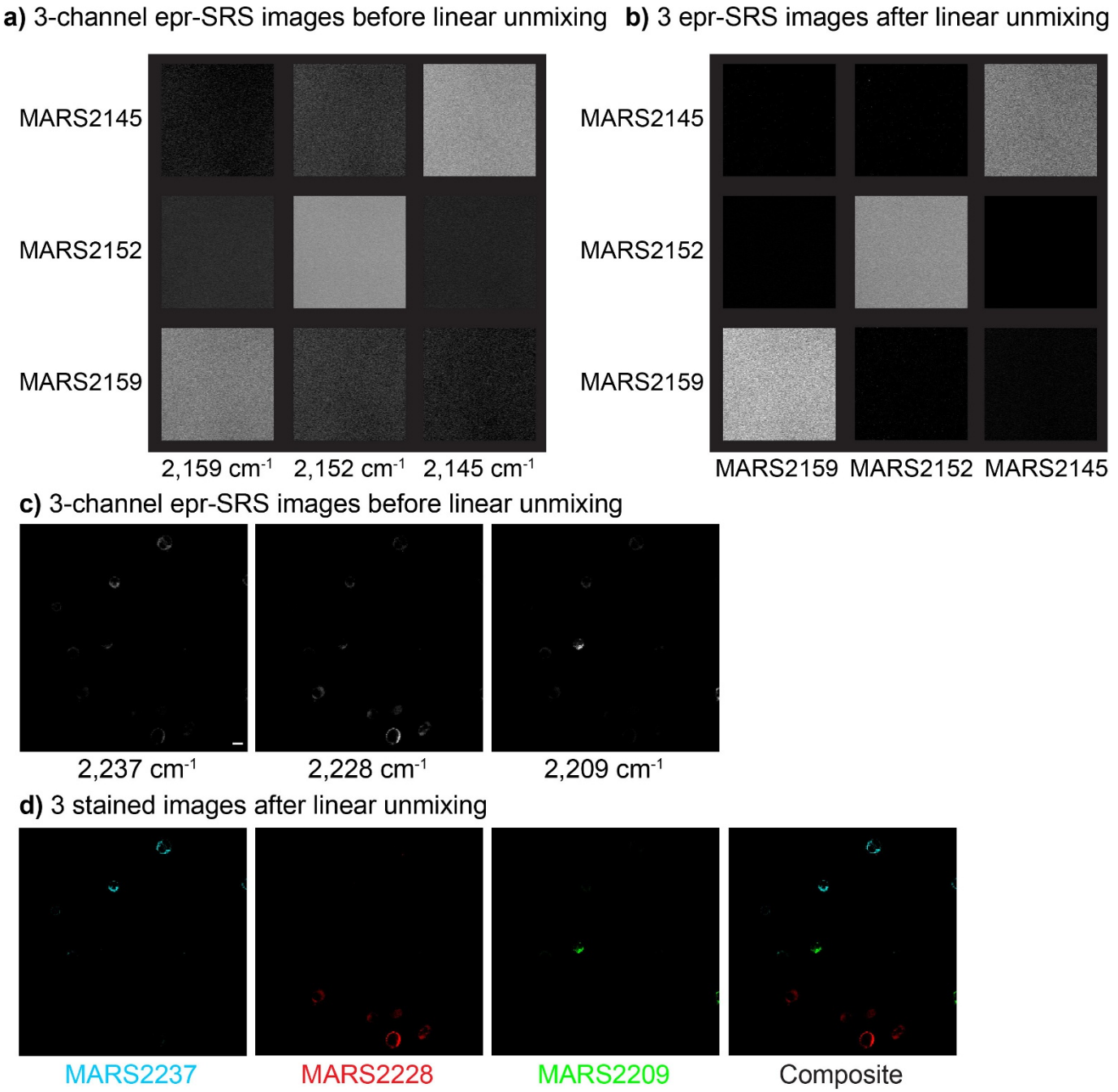

Extended Data Figure 7 | Linear unmixing on MARS solutions and MARS-dye-stained cells. a, Three-channel epr-SRS images at 2,159 cm^{-1}, 2,152 cm^{-1} and 2,145 cm^{-1} for 100 μM MARS2145, 1,000 μM MARS2152 and 300 μM MARS2159 before unmixing. **b**, Images after linear unmixing, with average readings of 94 μM, 1,097 μM and 315 μM for MARS2145, MARS2152 and MARS2159, respectively. **c**, Raw epr-SRS images for a 3-colour cell mix after each was stained with 1 μM MARS2237, 4 μM MARS2228 and 1 μM MARS2209 separately before linear unmixing. **d**, Images and their composite after linear unmixing.

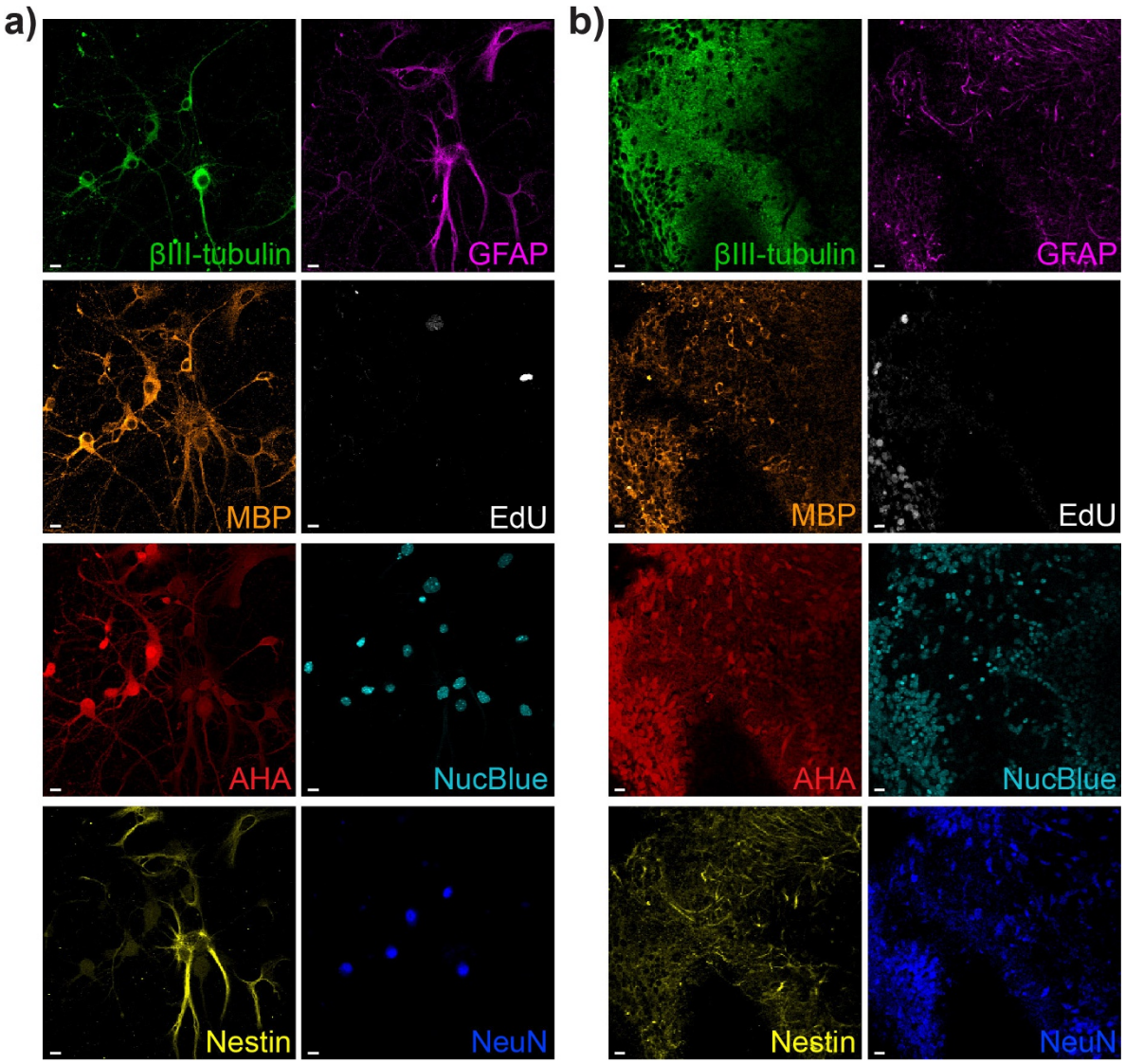

Extended Data Figure 8 | 8-colour epr-SRS and fluorescence imaging. a, **b**, Non-overlaid images of the hippocampal neuronal cultures shown in Fig. 4b (**a**) and the organotypic cerebellar brain slices shown in Fig. 4c (**b**). Scale bars, 10 μm.

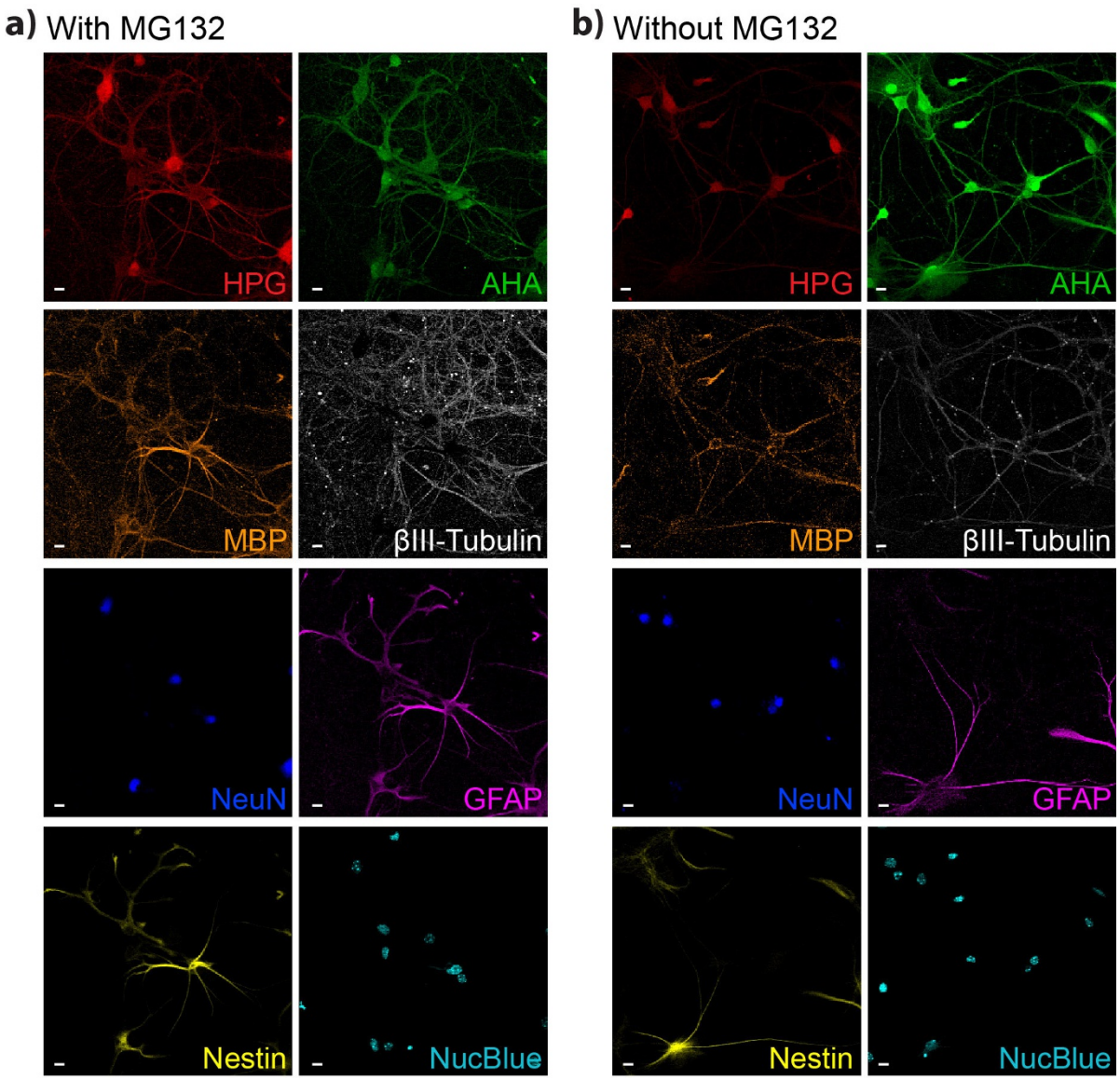

Extended Data Figure 9 | 8-colour epr-SRS and fluorescence imaging. a, **b**, Non-overlaid images of hippocampal neuronal cultures treated with MG132 as in Fig. 4d (**a**) and a control set without MG132 treatment (**b**). Scale bars, 10 μm.

Extended Data Table 1 | Raman cross-sections of 28 commercial dyes and their molecular absorption peaks across a large energy range

Name	Commercial source	λ_{max} (nm)	Double bond Raman Peak (cm^{-1})	Raman cross section (cm^2)*	S/B ratio	Solvent
Benzotriazole	B11400, Sigma	262	1,394	8.1×10^{-30}	20	a
Coumarin 153	546186, Sigma	430	1,604	2.1×10^{-28}	6	b
Rhodamine 6G	83697, Sigma	532	1,656	6.8×10^{-28}	40	a
Rhodamine B	83689, Sigma	558	1,659	1.1×10^{-27}	15	a
Sulforhodamine 101	S7635, Sigma	590	1,659	2.4×10^{-27}	60	d
Alexa633	A20105, Invitrogen	630	1,653	8.4×10^{-27}	19	d
Mitotracker deep red FM	M22426, Invitrogen	645	1,604	1.3×10^{-26}	5	e
CF640R	92085, Biotium	647	1,665	1.4×10^{-26}	10	d
Alexa647	A10277, Invitrogen	651	1,606	0.9×10^{-26}	2.5	d
Cy5	777323, Sigma	654	1,606	1.7×10^{-26}	4	d
DyLight650	62265, Thermo Scientific	658	1,606	1.0×10^{-26}	2.6	d
ATTO655	11774 Sigma	665	1,665	1.8×10^{-26}	10	d
Cyanine5.5	178, AAT-Bioquest	680	1,626	1.3×10^{-26}	2.2	d
Alexa680	A20008, Invitrogen	682	1,629	1.2×10^{-26}	1	d
ATTO-Oxa12	55785 SIGMA	682	1,659	2.3×10^{-26}	3.5	b
ATTO665	04022 SIGMA	682	1,641	2.3×10^{-26}	60	b
ATTO680	94875 Sigma	686	1,662	2.2×10^{-26}	75	b
Methylene Blue	M9140 Sigma	688	1,630	2.1×10^{-26}	21	b
Rhodamine800	83701 Sigma	700	1,652	2.9×10^{-26}	84	b
ATTO700	30674, Sigma	708	1,657	3.3×10^{-26}	40	b
Alexa700	A20010, Invitrogen	718	1,625	1.6×10^{-26}	1.8	b
ATTO725	47156 Sigma	744	1,640	7.8×10^{-26}	78	b
ATTO740	91394 Sigma	760	1,642	1.4×10^{-25}	80	b
3,3′-Diethylthiatricarbocyanine iodide	381306 Sigma	762	1,671	1.4×10^{-25}	5	c
Alexa750	A20011, Invitrogen	772	1,604	0.6×10^{-25}	1.4	b
Sulfo-Cyanine7	15320, Lumiprobe	774	1,622	1.5×10^{-25}	1.5	b
Cyanine7.5	A6030, Lumiprobe	800	1,628	1.9×10^{-25}	0.5	b
IR820	543365 Sigma	840	1,628	5.8×10^{-25}	0.3	b

The absolute Raman cross-section for C–O in methanol is $2.1\times10^{-30}\,cm^2$ at 785 nm (ref. 32) and is extrapolated to $0.9\times10^{-30}\,cm^2$ for our pump wavelength. Raman cross-sections are listed in reference to the C–O Raman cross-section in methanol. Solvents: a, water; b, DMSO; c, methanol; d, water + 5% DMSO; e, 50% water + 50% DMSO.

Extended Data Table 2 | Raman cross-sections of 22 MARS dyes

Name	λ_{max} (nm)	Triple bond Raman Peak (cm^{-1})	Raman cross section (cm^2)*	S/B ratio	Solvent
MARS2228	760	2,228	9.2×10^{-26}	12	DMSO
MARS2200	760	2,200	9.2×10^{-26}	8.8	DMSO
MARS2176	760	2,176	9.2×10^{-26}	11.2	DMSO
MARS2147	760	2,147	9.2×10^{-26}	9.5	DMSO
MARS2225	760	2,225	6.4×10^{-26}	10.5	DMSO
MARS2199	760	2,199	6.4×10^{-26}	10	DMSO
MARS2173	760	2,173	6.4×10^{-26}	8.5	DMSO
MARS2145	760	2,145	6.4×10^{-26}	10	DMSO
MARS2233	735	2,233	2.1×10^{-26}	30	DMSO
MARS2204	735	2,204	2.1×10^{-26}	33	DMSO
MARS2179	735	2,179	2.1×10^{-26}	38	DMSO
MARS2152	735	2,152	2.1×10^{-26}	42	DMSO
MARS2101	720	2,101	3.0×10^{-26}	5.5	AcOH
MARS2061	720	2,061	2.8×10^{-26}	6.5	AcOH
MARS2237	700	2,237	2.4×10^{-26}	62	DMSO
MARS2209	700	2,209	2.4×10^{-26}	70	DMSO
MARS2183	700	2,183	2.4×10^{-26}	80	DMSO
MARS2154	700	2,154	2.4×10^{-26}	60	DMSO
MARS2242	667	2,242	1.5×10^{-26}	8	DMSO
MARS2214	667	2,214	1.5×10^{-26}	9.2	DMSO
MARS2186	667	2,186	1.5×10^{-26}	8	DMSO
MARS2159	667	2,159	1.5×10^{-26}	9	DMSO

The absolute Raman cross-section for C–O in methanol is $2.1\times10^{-30}\,cm^2$ at 785 nm (ref. 32) and is extrapolated to $0.9\times10^{-30}\,cm^2$ for our pump wavelength. Raman cross-sections are listed in reference to the C–O Raman cross-section in methanol.